AD-A116 069 TENNESSEE UNIV SPACE INST TULLAHOMA F/G 9/2
ADAPTIVE CORRELATION CONCEPTS FOR NON-COMPATIBLE IMAGERY.(U)
OCT 81 L J PINSON, J C SU AFOSR-80-0275
UNCLASSIFIED AFOSR-TR-82-0484 NL

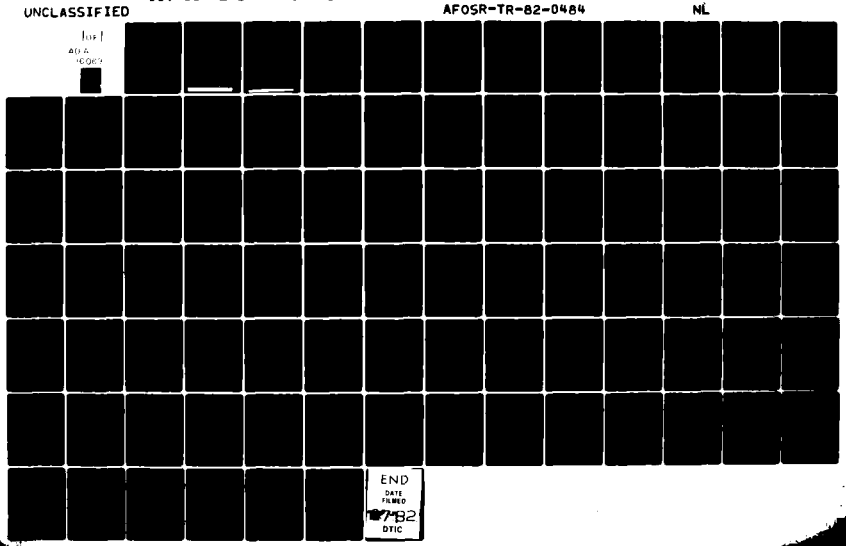

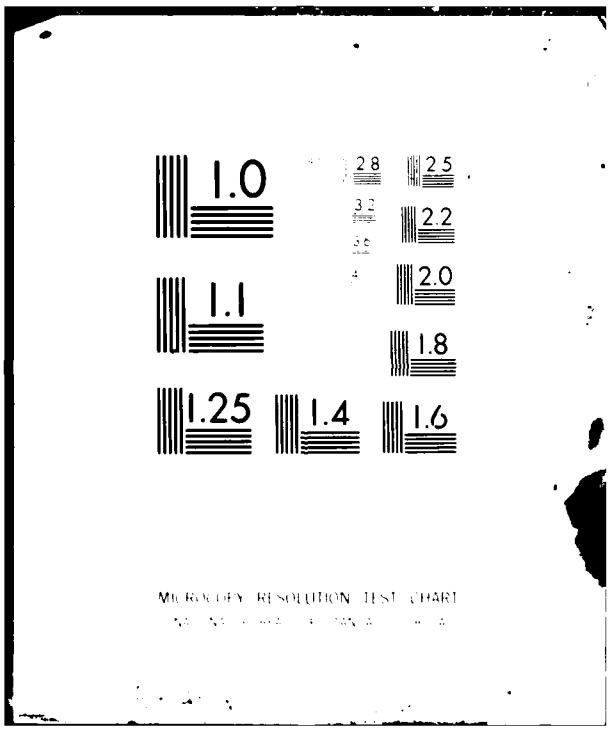
1.0
2.8
2.5
3.2
2.2
2.0
1.1
1.8
1.25
1.4
1.6
MICROCOPY RESOLUTION TEST CHART

ADAPTIVE CORRELATION CONCEPTS FOR NON-COMPATIBLE IMAGERY

Lewis J. Pinson & J. C. Su
University of Tennessee Space Institute
Tullahoma, TN 37388

31 October 1981

Final Technical Report

Unlimited Distribution

Prepared for

Air Force Office of Scientific Research

Bolling AFB, D.C. 20332

REPORT NUMBER **AFOSR-TR- 82-0484**	2. GOVT ACCESSION NO. AD-A116 019
	3. RECIPIENT'S CATALOG NUMBER
4. TITLE (and Subtitle) Adaptive Correlation Concepts for Non-Compatible Imagery	5. TYPE OF REPORT & PERIOD COVERED Final Technical 8-15-80 to 8-15-81
	6. PERFORMING ORG. REPORT NUMBER
7. AUTHOR(s) Lewis J. Pinson & J. C. Su	8. CONTRACT OR GRANT NUMBER(s) AFOSR-80-0275
9. PERFORMING ORGANIZATION NAME AND ADDRESS University of Tennessee Space Institute Tullahoma, TN 37388	10. PROGRAM ELEMENT, PROJECT, TASK AREA & WORK UNIT NUMBERS 61102F 2305/B2
11. CONTROLLING OFFICE NAME AND ADDRESS AFOSR/NE Bolling AFB, DC 20332	12. REPORT DATE 31 Oct 1981
	13. NUMBER OF PAGES 86
14. MONITORING AGENCY NAME & ADDRESS(if different from Controlling Office)	15. SECURITY CLASS. (of this report) Unclassified
	15a. DECLASSIFICATION/DOWNGRADING SCHEDULE

16. DISTRIBUTION STATEMENT (of this Report)

Approved for public release; distribution unlimited.

17. DISTRIBUTION STATEMENT (of the abstract entered in Block 20, if different from Report)

18. SUPPLEMENTARY NOTES

19. KEY WORDS (Continue on reverse side if necessary and identify by block number)
correlation, adaptive, non-compatible images, registration, preprocessing, quantization, thresholds, statistical characterization

20. ABSTRACT (Continue on reverse side if necessary and identify by block number)

As a result of characterizing joint scene content in terms of the joint probability density function, a new registration metric was defined as the thresholded difference (TD) method. It produced a sharper correlation peak than other pixel-by-pixel methods investigated. Analytical comparisons and simulations were done to show the effects of scene content on registrations by direct cross correlation, mean absolute difference and thresholded difference methods.

DD FORM 1 JAN 73 1473 EDITION OF 1 NOV 65 IS OBSOLETE

SECURITY CLASSIFICATION OF THIS PAGE (When Data Entered)

Block 20 (cont)

An adaptive binary quantizer was implemented which sets the quantization threshold as the mean or median in a 3 x 3 moving window. It showed far superior peak sharpness when compared with a global thresholding method; however, it showed greater sensitivity to noisy images.

Gradient pre-processing to enhance image high frequency content produced sharper correlation peaks for all methods except the TD method which was unaffected but still had the sharpest correlation peak of any method.

Simulations were done for imagery representing different spectral bands, different time of day and different scale. For these non-compatible images, the TD method showed results which were generally as good or better than the other methods.

SECURITY CLASSIFICATION OF THIS PAGE(When Data Entered)

SUMMARY

As a result of characterizing joint scene content in terms of the joint probability density function, a new registration metric was defined as the thresholded difference (TD) method. It produced a sharper correlation peak than other pixel-by-pixel methods investigated. Analytical comparisons and simulations were done to show the effects of scene content on registrations by direct cross correlation, mean absolute difference and thresholded difference methods.

An adaptive binary quantizer was implemented which sets the quantization threshold as the mean or median in a 3 x 3 moving window. It showed far superior peak sharpness when compared with a global thresholding method; however, it showed greater sensitivity to noisy images.

Gradient pre-processing to enhance image high frequency content produced sharper correlation peaks for all methods except the TD method which was unaffected but still had the sharpest correlation peak of any method.

Simulations were done for imagery representing different spectral bands, different time of day and different scale. For these non-compatible images, the TD method showed results which were generally as good or better than the other methods.

PREFACE

This final technical report describes the objectives, methods and results of contract AFOSR-80-0275 on "Adaptive Correlation Concepts for Non-Compatible Imagery" and covers the period 15 Aug 1980 to 15 Aug 1981. This effort was conducted by the Gas Diagnostics Research Division of The University of Tennessee Space Institute, Tullahoma, Tennessee 37388. It was sponsored by the U.S. Air Force Office of Scientific Research, Bolling AFB, DC 20332.

The authors wish to express their appreciation to Dr. John Neff of AFOSR for his support and to Mr. Ron Kaehr of Wright Patterson AFB, Ohio for his interest in this effort. Appreciation is extended to the U.S. Army Missile Command for providing imagery used in the simulations. And finally a special note of thanks to Sandy Shankle for her excellent assistance in manuscript preparation.

TABLE OF CONTENTS

page

SUMMARY iii
PREFACE iv
TABLE OF CONTENTS v
LIST OF ILLUSTRATIONS vii
LIST OF TABLES ix

1. INTRODUCTION AND SUMMARY 1
   1.1 Problem Statement and Objectives 2
   1.2 Proposed Effort 6
   2.3 Results Summary 9
      1.3.1 Thresholded difference algorithm . . . 9
      1.3.2 Gradient preprocessing 11
      1.3.3 Adaptive quantization threshold . . . 11

2. SCENE CHARACTERIZATION 11
   2.1 Scene Content and Correlation Accuracy . . . 12
   2.2 Statistical Characterization 12
      2.2.1 Simple moments and univariate statistics 13
      2.2.2 Joint statistical description 14

3. REGISTRATION METRICS 19
   3.1 Direct Cross-Correlation 19
   3.2 Mean Absolute Difference 21
   3.3 Thresholded Difference 22

4. PREPROCESSING AND QUANTIZATION 25
   4.1 Binary and Tri-level Quantization 25
   4.2 Adaptive Binary Quantizer 26
   4.3 Gradient Processing 27
   4.4 Gain and Mean Correction 28

5. SIMULATION RESULTS 29
5.1 Scene Descriptions 31
5.2 Metric Comparison 35
5.3 Noise Effects on Registration Peak 45
5.4 Gradient Preprocessed Images 50
5.5 Adaptive Quantizer 50
5.6 Non-Compatible Images 58
5.6.1 Different spectral bands 61
5.6.2 Different time of day 62
5.6.3 Different scale 67

6. CONCLUSIONS AND RECOMMENDATIONS 75

REFERENCES 77

LIST OF ILLUSTRATIONS

Figure	Description	Page
1.1	Concepts for Correlator Evaluation	10
2.1	Joint Histogram Properties	16
2.2	Joint Gaussian pdf	18
3.1	Properties of Images for Registration . . .	20
3.2	Effect of Binary and Tri-level Quantization on Correlation as Represented by the Joint pdf Between r and s	23
3.3	Thresholded Difference Method	24
4.1	Binary and Tri-level Quantizers	25
4.2	Gain and Mean Errors in Joint Histogram Domain	28
5.1	Simulation Options Summary	30
5.2	Image Segments from Silicon TV	33
5.3	Ohio Files 2 and 10 Image Segments	33
5.4	Ohio Files 26 and 27 Image Segments	34
5.5	HSV Files 9 and 10 Image Segments	35
5.6	Scene 1, Vertical Profiles Through Peak (Noise-free)	37
5.7	Thresholded Difference, Scene 1, Vertical (Noise-free).	38
5.8	Scene 1, Horizontal Profiles Through Peak (Noise-free).	39
5.9	Thresholded Difference, Scene 1, Horizontal (Noise-free).	40
5.10	Scene 2, Vertical Profiles Through Peak (Noise-free).	41
5.11	Thresholded Difference, Scene 2, Vertical (Noise-free).	42
5.12	Scene 2, Horizontal Profiles Through Peak (Noise-free).	43
5.13	Thresholded Difference, Scene 2, Horizontal (Noise-free).	44
5.14	Scene 1, Additive Noise (S/N=0.43) (Vertical)	46

5.15 Scene 1, Additive Noise (S/N=1.42) (Vertical) 47
5.16 Scene 1, Vertical Profile, Gradient (Noise-free) 51
5.17 Scene 1, Horizontal Profile, Gradient (Noise-free) 52
5.18 Scene 2, Vertical Profile, Gradient (Noise-free) 53
5.19 Scene 2, Horizontal Profile, Gradient (Noise-free) 54
5.20 Scene 1, Vertical, 3 x 3 Mean Adaptive . . . 56
5.21 Scene 1, Horizontal, 3 x 3 Mean Adaptive 57
5.22 Scene 1, Vertical, 3 x 3 Median Adaptive 59
5.23 Scene 1, Horizontal, 3 x 3 Median Adaptive 60
5.24 Different Spectral Bands (Vertical, Ohio Files 26,27) 63
5.25 Different Spectral Bands (Horizontal, Ohio Files 26,27) 64
5.26 Different Spectral Bands, Gradient (Vertical, Ohio Files 26,27) 65
5.27 Different Spectral Bands, Gradient (Horizontal, Ohio Files 26,27) 66
5.28 Different Time of Day (Vertical, Ohio Files 2,10) 68
5.29 Different Time of Day (Horizontal, Ohio Files 2,10). 69
5.30 Different Time of Day, Gradient (Vertical, Ohio Files 2,10). 70
5.31 Different Time of Day, Gradient (Horizontal, Ohio Files 2,10). 71
5.32 Different Scale & Spectral Bands (Vertical, HSV Files 10,9) 73
5.33 Different Scale & Spectral Bands (Horizontal, HSV Files 10,9) 74

LIST OF TABLES

Table No.	Description	Page
5.1	Scene Descriptions	32
5.2	Noise Effects	49
5.3	Noise Effects on Adaptive Threshold Method Peak Location	58
5.4	Results for Different Spectral Band	61
5.5	Results for Different Time of Day	62
5.6	Results for Different Scale	72

1. INTRODUCTION AND SUMMARY

A number of Air Force systems, whose operating regimes include mid-course and terminal phases, have need for reliable, stand-alone guidance capability. A useful technique for accomplishing this guidance has been to correlate imagery from an on-board sensor with reference imagery stored in a computer.

The development of smaller, faster and less expensive signal processing hardware makes it practical to consider in more detail the possibility of real-time or near real-time processing of two-dimensional data sets such as obtained from sensors in multiple spectral bands. Further it is possible to consider doing more of this processing on-board to reduce dependence on data links. Applications for real-time two-dimensional processing of imagery include image registration, automatic target handoff, pattern recognition and feature extraction. The major technique for accomplishing these applications is computation of the cross-correlation function between a reference image and the incoming, unclassified imagery.

The remainder of this section provides a summary of the problem statement and objectives, details of the effort proposed to accomplish those objectives, and a summary of significant results. Further details of the method and results are given in sections 2. through 6.

1.1 Problem Statement and Objectives. The correlation technique works well under ideal conditions, i.e., compatible sensors, no geometric distortion, high signal-to-noise ratio and relaxed time constraint for computation. In fact, a number of variations on the cross-correlation function algorithm have been shown to reduce false peaks, provide high spatial registration accuracy or reduce required computation time. Unfortunately the advantages mentioned above are usually competitive and not attainable with any one given algorithm. In many cases the two images are obtained from different sensors so that differences in field-of-view, spectral response and geometric distortion add to the processing complexity and introduce additional error sources in the cross-correlation technique.

Variations on the classical cross-correlation function definition have been examined which seek to improve resolution, reduce false peaks and increase processing speed. A technique known as the sequential similarity detection algorithm [1] increases processing speed by computing a function based on the difference of data point amplitudes instead of their product. Since subtraction is a faster process than multiplication, a time savings is realized. A phase correlation technique which improves resolution and false peak rejection is described by Kuglin and Hines [2]. Unfortunately this improved performance is achieved at the cost of increased processing complexity.

Algorithms which sacrifice gray-scale for increased processing speed are reported by various companies engaged in two-dimensional correlation research. These algorithms offer the best promise for real-time correlation of two images. In fact if an extreme coarse quantization (2 level or 1 bit) is used then multiplication and addition are reduced to simple logic functions. The sequential similarity detection algorithm and direct cross-correlation algorithms are then computationally equivalent, the only difference being in the specific logic operation required for implementation.

The effects of coarse quantization on correlation processes have been examined in detail elsewhere [3] - [7]. A brief summary statement of the results indicates that the statistical disadvantage incurred by coarse quantization of the images is offset by being able to include more pixels in the correlation computation for a real-time requirement, assuming that geometric distortion is not a problem. Thus for an application which requires real-time correlation, quantization of the data to two levels is an attractive technique. A more complete comparison of various correlation techniques for the automatic handoff problem is given in [6].

Examination of the probabilities of false registration and detection for correlation of two television images, as a function of the video signal-to-noise ratios and a preset correlation threshold, has been done for coarse quantization of the video signals to two levels [8].

Several approaches to the false acquisition problem have assumed gaussian statistics for the correlation function itself. Rockmore [9] extends this approach using an Edgeworth series expansion so that the correlation function statistics are no longer restricted to being gaussian.

Limited parametric analyses have been done by various investigators which show the effects on correlator performance of quantization method [7], image rotation, image scale differences, synchronization error [10] and image sampling masks for specific applications. These specific applications typically involve correlation of images from like sensors; and, the correlator performance is strongly influenced by individual scene statistics. A recent effort [11] has looked at the problem of correlating a day TV image with imagery from a co-located forward-looking infrared (FLIR) system. Such an approach to correlating imagery from different sensor types is important for development of an all-weather capability without requiring that a reference image be stored for each sensor. Individual scene statistics can be shown to strongly affect the probability of correct registration for any correlation algorithm. Some method for adjusting correlator thresholds or preprocessing steps adaptively, dependent on the scene statistics, is needed.

It is desirable to provide a sound theoretical base which shows dependence of correlator performance on all the above parameters in such a way that the results could be applied to new guidance concepts, including those using

non-compatible sensors in an all-weather system. Further, it is desirable to characterize ability of the correlator to automatically identify target classes and to reject similar false targets. Also, experimental validation of the theory by correlator simulation using actual multi-spectral imagery is desirable.

Based on familiarity with guidance concepts and sensors used in Air Force systems the following three objectives are stated for this effort.

Objective #1: Develop specific characterization of parametric effects on correlator performance in a way to provide maximum flexibility in application to existing and new system concepts. Parameters will include but not be limited to: quantization method, error sources, contrast reversals, threshold for quantization, threshold for correlation, non-compatible sensors and effect of selected pre-processing algorithms.

Objective #2: Characterize dependence of correlator performance on individual scene statistics for compatible and multi-sensor imagery. Develop theory for an adaptive correlator which optimizes performance for given scene statistics.

Objective #3: Using actual imagery, validate parametric dependence through computer implementation of various correlation and pre-processing algorithms.

1.2 Proposed Effort. Of the related areas essential to the development of an all-weather capability for guidance based on correlation of imagery, several are in need of further analysis and verification through simulation to improve correlator performance and to predict critical parametric dependence.

Several key points need to be examined and understood to provide a good measure of expected correlator performance for stand-alone, all-weather systems. These key points and several related problems will be examined in detail in the proposed program.

Specifically, solutions of the following problems are critical to meeting the desired objectives for an image correlation system:

1. Scene Dependence - Relative sharpness of the correlation function, probability of correct registration and the success of pre-processing algorithms have been shown through simulation studies to depend strongly on scene characteristics. This dependence must be characterized to allow optimization of correlator performance.
2. Threshold Effects - Both in terms of quantizer threshold and detection threshold, there are still uncertainties on how these values should be chosen. Further, thresholding for edge detection algorithms has a critical impact on correlator performance. A sound theoretical

base backed up by simulation results is needed to provide guidelines on threshold selection.

3. Pre-processing and Distortion - Further work is needed to determine the effects of distortion and what kinds of pre-processing would improve correlator performance. Specifically, in terms of images from non-compatible sensors there is a need to investigate algorithms in addition to the gradient method. A trade-off of correlator improvement versus computational burden must be developed for uniform comparison of processing methods.

4. Adaptive Correlation - Once parametric dependence for distortion, scene statistics, threshold effects and processing methods have been determined, it is desirable to provide an adaptive capability for the correlator to optimize performance.

5. All-weather Capability - All the above analyses and simulations should be based on conditions which would provide a stand-alone system with all-weather capability.

The following tasks are proposed for accomplishment of the goal of developing a model and methods for evaluating the parametric dependence of image registration performance.

Task 1: Gain familiarity with specific details of guidance concepts and sensors used in existing and planned Air Force Systems. This task will be accomplished by visits to Wright Patterson AFB.

Task 2: Example imagery for correlation analysis will be selected from available imagery from specific Air Force systems, from multi-spectral photographs digitized by scanning microdensitometer, or from computer-generated special case imagery of known statistics.

Task 3: Distortion including rotation and scale errors of selected magnitudes will be applied to the imagery. Effect on correlator performance will be quantified.

Task 4: Quantization effects on correlator performance will be evaluated for continuous gray scale, binary and 3-level quantizers showing effects of quantizer thresholds.

Task 5: Pre-processing algorithms which extract edge information from the imagery will be evaluated in terms of their effect on correlator performance measures.

Task 6: Scene characterization in terms of joint probability density functions will be computed for the sample imagery for selected distortions and pre-processing algorithms.

Other descriptive features will be computed for scene characterization.

Task 7: A sound theoretical base will be established for evaluating correlator performance in terms of scene characteristics, quantization method, selected distortions and pre-processing methods.

Task 8: Based on parametric analyses of correlator performance, adaptive methods for performance optimization will be recommended.

Figure 1.1 shows the concepts included in this proposed effort. The combined experimental/theoretical approach should provide definitive answers about the effects of specific parameters on correlator performance.

1.3 Results Summary. Early emphasis was placed on characterizing scene content and on utilizing scene content to adaptively modify the correlation approach (in choice of algorithm, quantization thresholds or preprocessing steps). Specific accomplishments are summarized below.

1.3.1 Thresholded difference algorithm. As a result of characterizing joint scene content in terms of the joint probability density function a new registration metric was defined (referred to in this report as the thresholded difference (TD) method) which provides a sharper correlation peak than any other pixel-by-pixel method investigated. Because of this promising performance the effort was redirected to provide a more thorough analysis of the TD method.

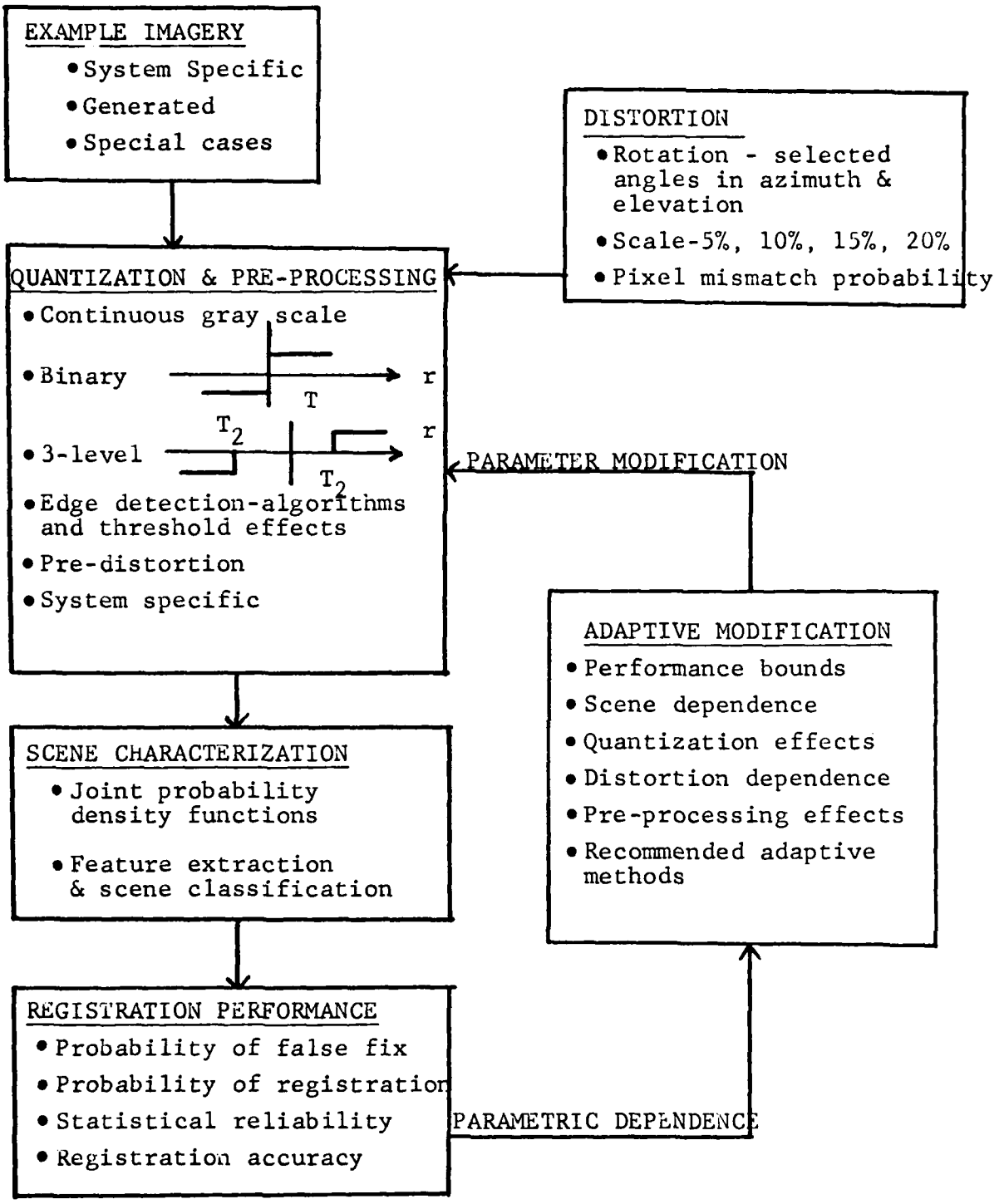

Figure 1.1 Concepts for correlator evaluation

1.3.2 Gradient preprocessing. Since images with higher spatial frequency content produce sharper correlation peaks, it follows that a high frequency emphasis processor such as the gradient should produce a sharper correlation peak. A simple 3 x 3 gradient processor was applied to typical TV and FLIR imagery. The resultant correlations were sharper for all algorithms except the TD method which was still the sharpest peak of all. Since the TD method is inherently a high resolution method anyway, then gradient processing had little or no effect on it.

1.3.3 Adaptive quantization threshold. For binary and tri-level correlators the quantization thresholds are typically chosen to be dependent on global scene statistics (mean and standard deviation). This global thresholding tends to reduce high spatial frequencies in the image, even for images which have been gradient processed. A locally adaptive quantization method was implemented whereby thresholds are based on statistics (mean and standard deviation) within a small window about the pixel being quantized. Simulation results for a binary correlator using an adaptive threshold in a 3 x 3 window gave a high resolution correlation function.

2. SCENE CHARACTERIZATION

One objective for this effort was to develop methods for characterizing scene content and to make use of knowledge of scene content to optimize registration algorithms, parameters, etc.

2.1 Scene Content and Correlation Accuracy. One measure of scene content is its two-dimensional spatial transform which gives a detailed measure of spatial frequency content in the image. From two images r and s, whose transforms are R and S, we form the two-dimensional cross spectrum of spatial frequency.

$$G_{RS}(\beta,\partial) = R(\beta,\partial)\, S^{*}(\beta,\partial) \qquad (2\text{-}1)$$

The inverse transform of G is the cross correlation function, C, of r and s.

$$C_{rs}(\alpha,\delta) \overset{F}{\Longleftrightarrow} G_{RS}(\beta,\partial) \qquad (2\text{-}2)$$

Further, because of the inverse relationship of size between two Fourier domains, it follows that high spatial frequencies in G transform to sharp correlation peaks in C. Therefore, a sharper, more accurate correlation peak is expected from imagery with high spatial frequency content; and, preprocessing algorithms which enhance high frequencies have the potential for improved correlator performance.

2.2 Statistical Characterization. One method for concise characterization of scene content is in terms of statistical descriptions. Univariate statistics give a description of individual images and bivariate statistics provide joint descriptions between images. In either case, the most complete statistical description is provided by estimates for the n-th order probability density functions (pdf). Other statistical descriptors such as moments or statistical functions can be defined in terms of the appropriate pdf.

2.2.1 Simple moments and univariate statistics. Mean and standard deviation are often used as parameters in setting quantization thresholds for binary and tri-level registration methods. These parameters are estimated as array averages for an image, f, with K x L pixels as

Mean estimate

$$\hat{\mu} = \frac{1}{KL} \sum_{i=1}^{K} \sum_{j=1}^{L} f(i,j) \tag{2-3}$$

Standard deviation estimate

$$\hat{\sigma} = \left[\frac{1}{KL-1} \sum_{i=1}^{K} \sum_{j=1}^{L} \left(f(i,j) - \hat{\mu} \right)^2 \right]^{\frac{1}{2}} \tag{2-4}$$

Additional statistical descriptions for the image are given by the following functions.

1. Histogram - an estimate for the univariate amplitude probability density function (for 8 bit quantization)

$$h(a) = \frac{n_a}{KL} \qquad a = 0,255 \tag{2-5}$$

n_a = number of pixels at amplitude a

2. Fourier spectrum

$$G_{ff}(\beta,\partial) = \left| FFT\{f(x,y)\} \right|^2 \tag{2-6}$$

3. Autocorrelation function

$$C_{ff}(\alpha,\delta) = IFFT\left[G_{ff}(\beta,\partial) \right] \tag{2-7}$$

2.2.2 Joint statistical description. Registration properties of two images are completely characterized by the joint probability density function between the two images with shift in two dimensions (α,δ) as parameters. Parametric analysis of this joint pdf requires knowledge of the cross correlation function between the two images. Since the objective is to use the joint pdf to predict cross correlation properties, the analytical approach appears to go in circles.

An estimate for the joint pdf between two images is given by their joint histogram. For eight-bit images the joint histogram has a domain of 256 x 256 values and presents a relatively complicated statistical description of the joint properties of the two images. Additionally a complete histogram surface is generated for each relative spatial shift between the two images. Thus it appears that characterizing two images by their joint histograms is a formidable task which produces too much information to be useable. Strictly speaking this is true; however, there is useful information and enhanced understanding to be achieved from examining the joint histogram.

For images r and s with 8-bit pixel values and size K x L, the joint histogram for shift (α,δ) is given by

$$h(a,b,\alpha,\delta) = \frac{n(r_a,s_b)}{KL} \qquad a,b = 0,255 \qquad (2\text{-}8)$$

where $n(r_a,s_b)$ = number of pixel pairs
wherein the amplitude in r was a
while the amplitude in s was b.

Some insight into the registration process is achieved by examining the properties of the joint histogram for some special cases. At registration, ideally, all pixels match exactly and all points in the joint histogram lie along the r=s line as shown in figure 2.1a.) Realistically, at registration some pixels will not match due to uncorrelated noise in the images or due to geometric distortions. These mismatched pixels are represented as points scattered off the r=s line in figures 2.1b.) and c.). The rms scattering distance is relatable to signal-to-noise ratio or to percent distortion.

The effects of gain errors and mean value shifts between the two images are illustrated in figures 2.1 d.), e.) and f.). It will be shown later that these two errors may be corrected by a simple amplitude range scaling prior to registration.

Further insight into the behavior of the joint pdf for two images with varying degrees of correlation is gained by examining the special case where r and s are jointly gaussian. Equi-amplitude contours in the joint pdf domain are shown in Figure 2.2 for a) uncorrelated-equal variance; b) uncorrelated-unequal variance; c) partially correlated; and d) correlated (perfectly registered).

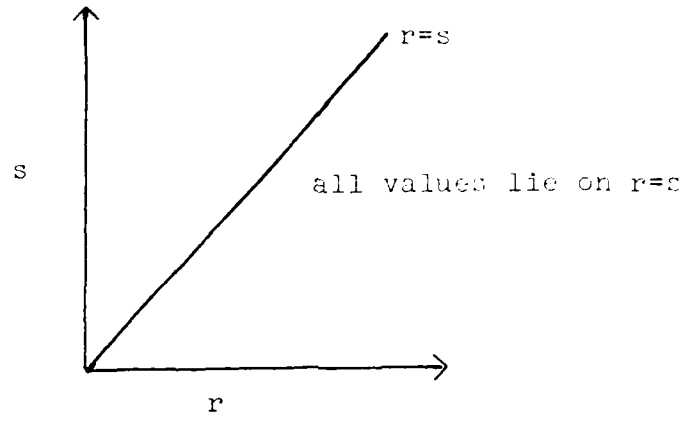

a.) Ideal registration

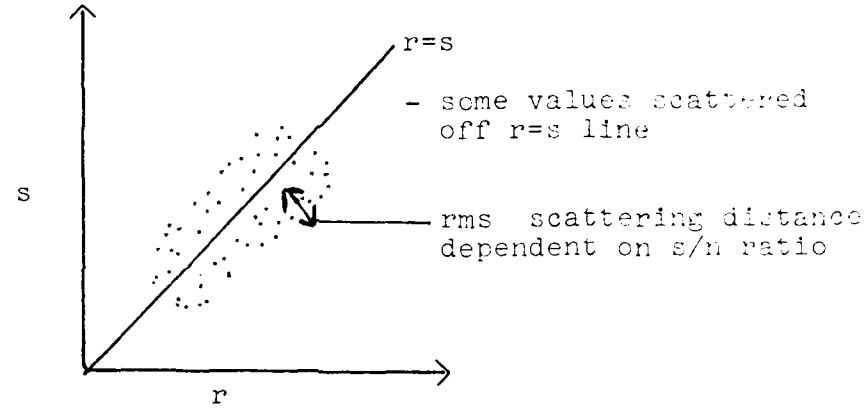

b.) Uncorrelated noise at registration

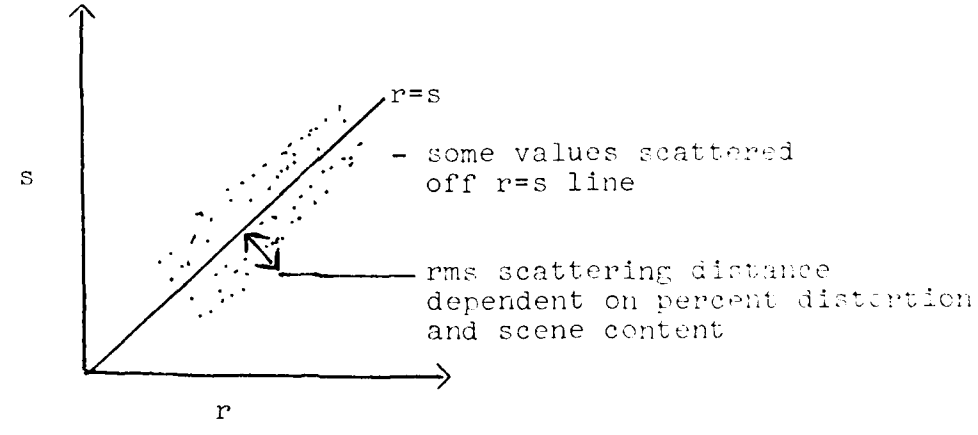

c.) Geometric distortion at registration

Figure 2.1 Joint Histogram Properties

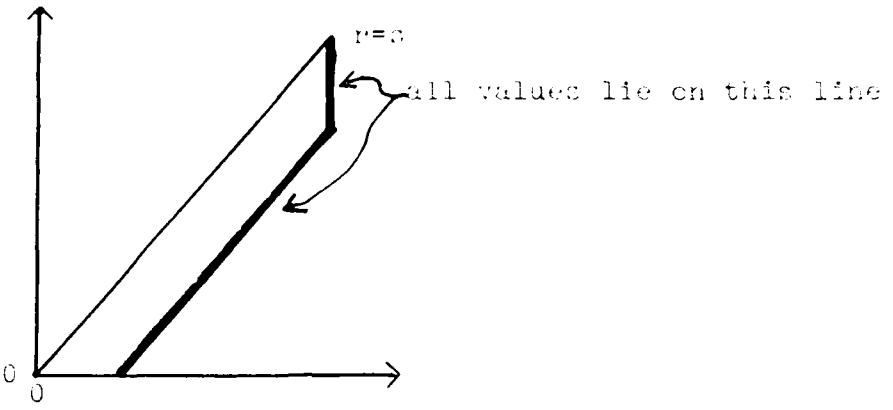

d.) Mean value shift at registration

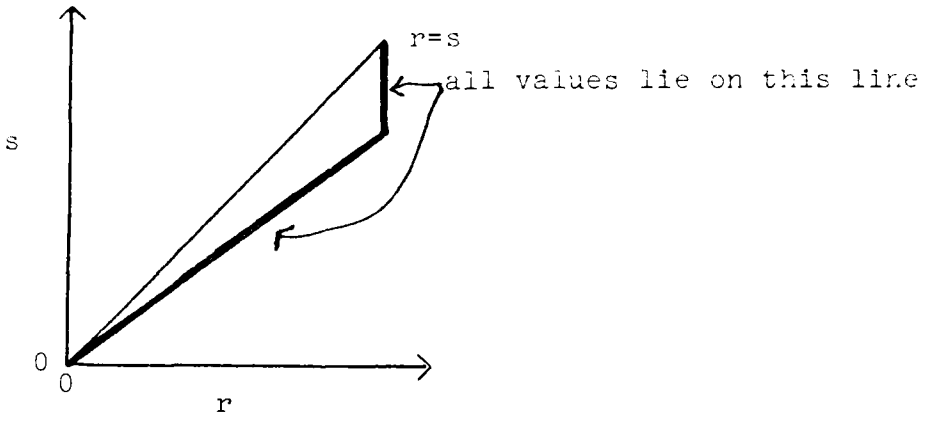

e.) Gain error at registration

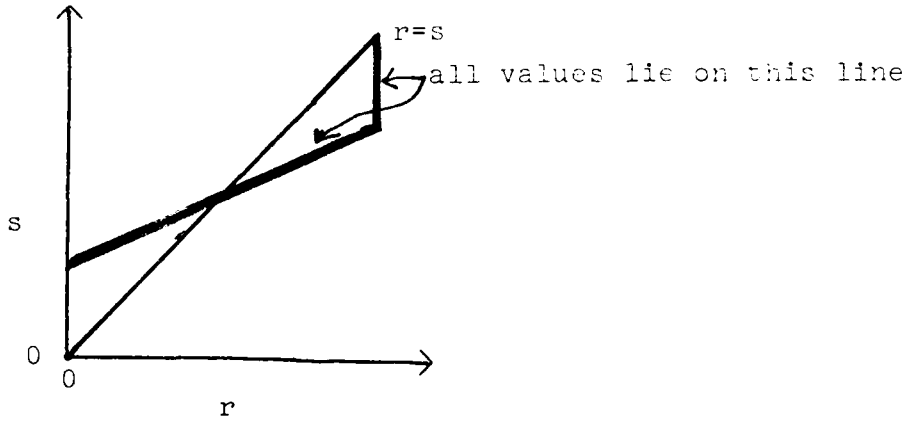

f.) Gain error and mean value shift at registration

Figure 2.1 (cont'd)

JOINT HISTOGRAM

IF r & s ARE JOINT GAUSSIAN

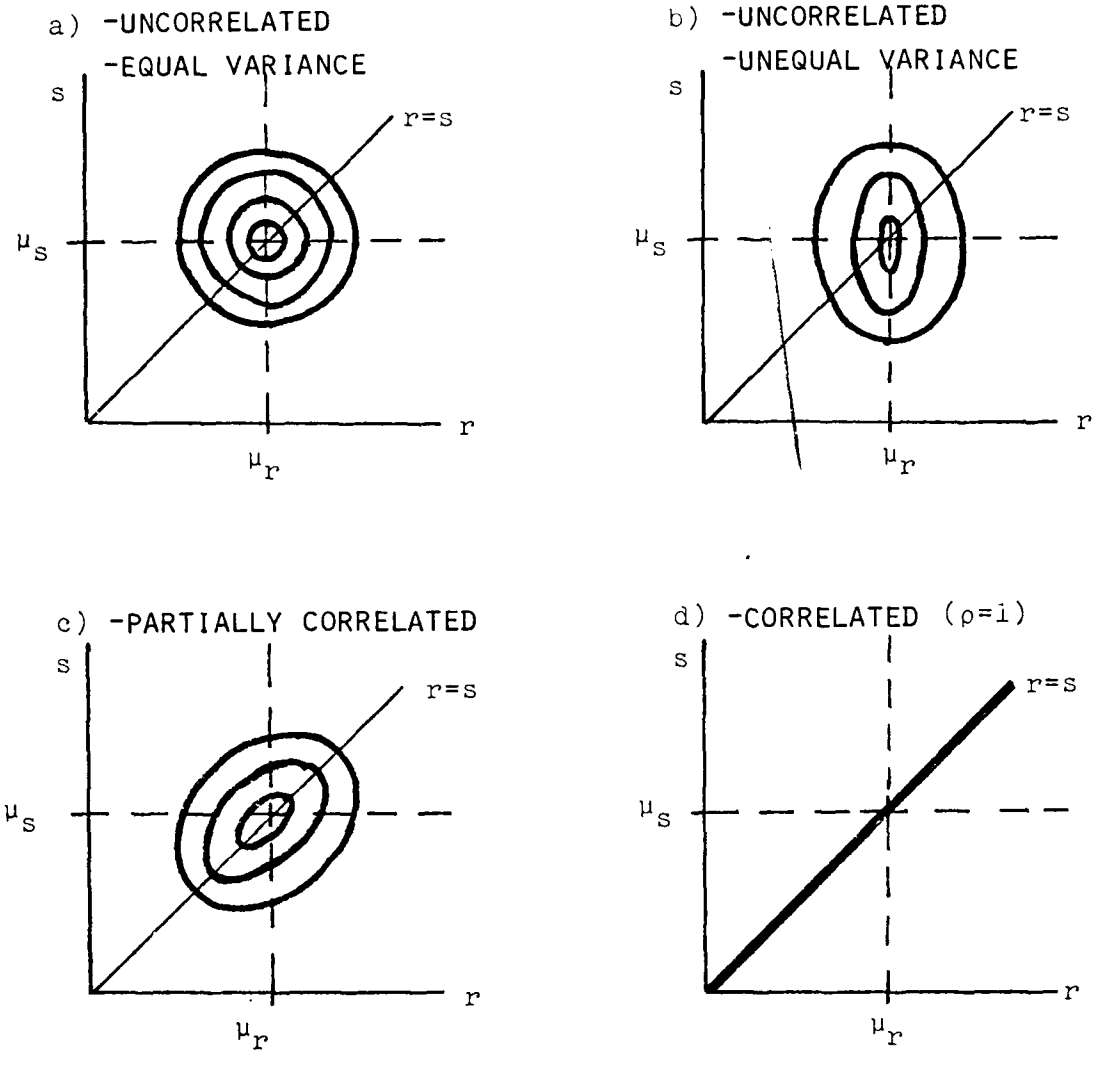

AT REGISTRATION - IDEALLY r=s

Figure 2.2 Joint Gaussian pdf

3. REGISTRATION METRICS

There are several registration metrics which may be defined for comparing two images [6] and [12]. Three metrics were investigated and compared as part of this effort. The "direct cross correlation" and "mean absolute difference" metrics were included because of their widespread use in real-time or near real-time applications. The "thresholded difference" metric was developed as part of this effort. Definitions and properties for these three metrics are given in this section.

Definitions are given for correlating two images r and s of size K x L and M x N pixels respectively as shown in Figure 3.1. Shift values (p,q) are restricted so that the images always have KL overlapping pixels.

3.1 Direct Cross Correlation. The definition for the discrete cross correlation between two spatial functions $f_1(n,m)$ is given by (3-1)

$$C(p,q) = E\left[f_1(n,m)\ f_2(n+p,\ m+q)\right] \qquad (3\text{-}1)$$

where:

$E\left[\bullet\right]$ is expected value

Based on an image model which is characterized by a shift-variant mean and shift-invariant second-order statistics [12], (3-1) may be estimated from a spatially averaged function. Equation (3-2) defines a nomalized direct cross correlation (DCC) algorithm for estimating C(p,q) for the image models shown in Figure 3.1.

GIVEN - OBJECT OF INTEREST IS CENTERED IN $r(m,n)$
- OBJECT OF INTEREST IS WITHIN $s(m,n)$

OBJECTIVE - LOCATE OBJECT IN $s(m,n)$ and find p^*, q^*

AFTER SCALE MATCHING

$s(m,n)$ has M x N pixels
$r(m,n)$ has K x L pixels

SHIFT VALUES

$p = 0, 1, -----, M-K$
$q = 0, 1, -----, N-L$

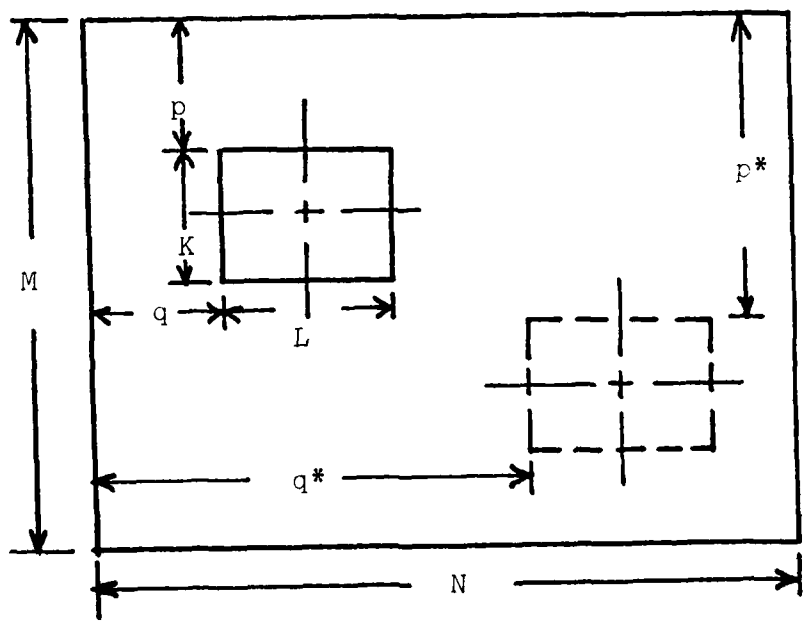

Figure 3.1 Properties of Images for Registration

$$\hat{C}_{rs}(p,q) = \frac{\sum_{m=1}^{K}\sum_{n=1}^{L} r(m,n)s(m+p,n+q)}{\left\{\left[\sum_{m=1}^{K}\sum_{n=1}^{L} r^2(m,n)\right]\left[\sum_{m=1}^{K}\sum_{n=1}^{L} s^2(m+p,n+q)\right]\right\}^{1/2}} \qquad (3\text{-}2)$$

where: $p = 0, M-K$

$q = 0, M-L$

For quantization of r and s to 1 bit (2 levels) or ± 1, the denominator term in (3-2) reduces to KL to give

$$\hat{C}_{rs}(p,q) = \frac{1}{KL}\sum_{m=1}^{K}\sum_{n=1}^{L} r(m,n)s(m+p, n+q) \qquad (3\text{-}3)$$

Both (3-2) and (3-3) have the property that $\hat{C} = 1$ at registration.

3.2 Mean Absolute Difference. The definition of the mean absolute difference algorithm (MAD) for the images in Figure 3.1 is given by equation (3-4).

$$\hat{E}_{rs}(p,q) = 1 - \frac{1}{KL}\sum_{m=1}^{K}\sum_{n=1}^{L} \left| r(m,n) - \bar{r} - s(m+p,n+q) + \bar{s}_{pq} \right| \qquad (3\text{-}4)$$

where $\bar{r}$ is the mean value of r

$$\bar{r} = \frac{1}{KL}\sum_{m=1}^{K}\sum_{n=1}^{L} r(m,n) \qquad (3\text{-}5)$$

and $\bar{s}_{pq}$ is the mean value of KL pixels in s at shift p,q.

$$\bar{s} = \frac{1}{KL}\sum_{m=1}^{K}\sum_{n=1}^{L} s(m+p,n+q) \qquad (3\text{-}6)$$

As defined in (3-6) the DAD algorithm gives a measure of [illegible] at registration (locally). For binary quantization [illegible] s about their respective mean values and [illegible] with values between 0 and 1 for $\hat{r}$ [illegible]

$$\hat{E}_{rs}(i,j) = 1 - \frac{1}{KL} \sum_{m=1}^{K} \sum_{n=1}^{L} \left| r(m,n) - s(m+i, n+j) \right| \qquad (3-7)$$

Direct comparison of (3-6) and (3-7) [illegible], for binary quantization, to [illegible].

3.3 Threshold Difference. The threshold difference algorithm was developed from two [illegible]:

1. Because of an emphasis on reduced [illegible], the binary and tri-level quantized [illegible] algorithms were examined for potential [illegible],
2. Because of an emphasis on simplicity [illegible], the DCD and MAD algorithms were examined in terms of the joint probability density [illegible]
3. From these considerations the [illegible] was developed as an heuristically obvious improvement.

For the binary and tri-level DCD and MAD algorithms, the r and s are subjected to independent quantization with one threshold for binary and two thresholds for tri-level quantization. These thresholds are usually derived from [illegible] standard deviation values in each image. In terms of the joint probability density function between r and s, the situation shown in Figure 3.2 results.

The cross-hatched regions represent values of r and s which will be considered to be matched by the binary and tri-level correlators. At registration, ideally, all values should lie along the r=s line in the joint pdf domain.

DOMAIN OF JOINT PROBABILITY DENSITY

QUANTIZERS

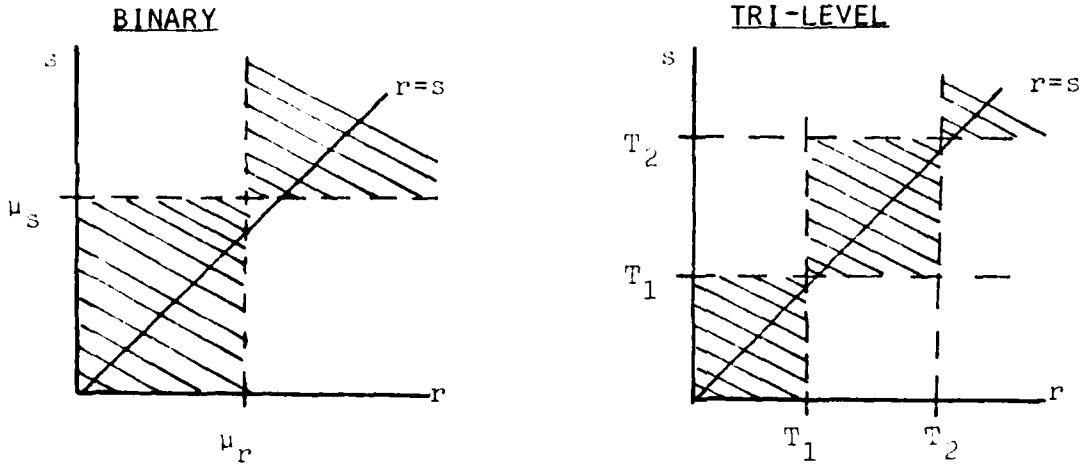

Figure 3.2 Effect of Binary and Tri=level Quantization on Correlation as Represented by the Joint pdf Between r and s.

It is clear that there are areas where exact or near matches are counted as non-matches by the two methods; and, there are areas where r and s have widely different values that are counted as matches.

A more logical approach is to consider two pixels as matched if their values agree within some specified threshold centered about the r=s line. The result is shown in Figure 3.3a) in terms of the joint pdf and a simple implementation is shown in Figure 3.3 b).

The thresholded difference algorithm is computationally equivalent to the 8-bit MAD algorithm except that the magnitude error is thresholded. This allows for small (specifiable) errors between amplitudes of r and s with no penalty. The resultant metric should exhibit a sharper registration peak. Simulation results presented in section 5. verify this hypothesis.

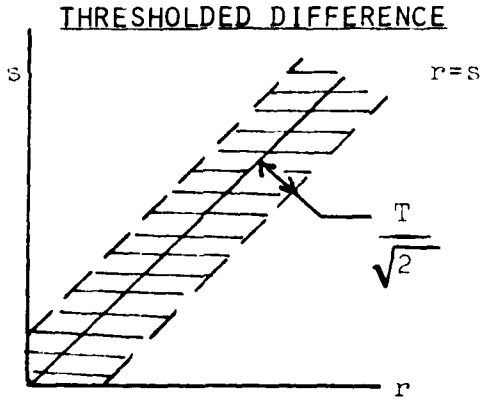

a) Representation in joint pdf domain

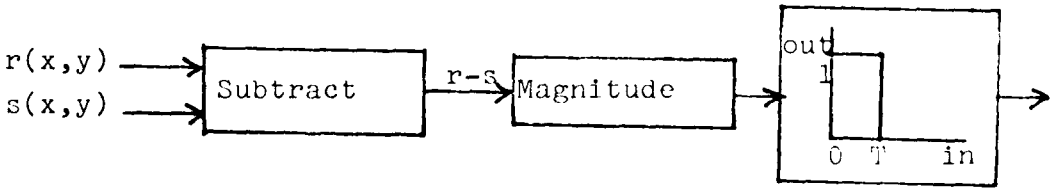

b) Implementation

Figure 3.3 Thresholded Difference Method

4. PREPROCESSING AND QUANTIZATION

There are numerous preprocessing methods with potential for application to the registration problem. For this effort, methods used in simulations were kept simple and selected with the goal of improving correlation peak sharpness. Relatively simple statistically based thresholds were defined for the binary and tri-level quantizers.

Gradient preprocessing was implemented to enhance high frequency content in the images and produce a sharper correlation peak. A locally adaptive method was implemented for the binary quantizer.

Preprocessing to correct for mean value shift and gain differences for pixel amplitudes for the two images is important if good results are to be obtained with the thresholded difference method.

These preprocessing methods are discussed in this section.

4.1 Binary and Tri-Level Quantization. The images were quantized to two levels or three levels as shown in Figure 4.1.

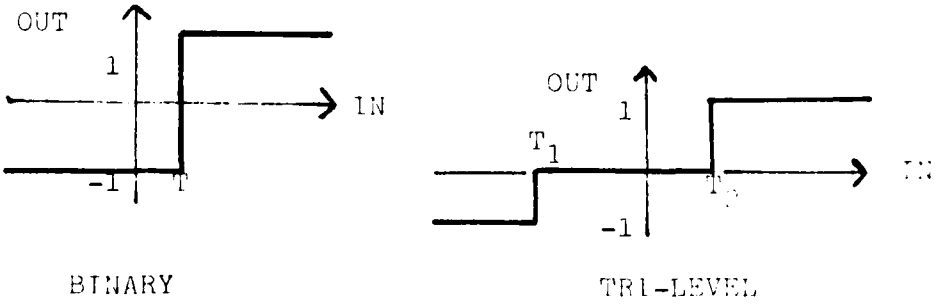

Figure 4.1 Binary and Tri-level Quantizers

For the images, thresholds were defined in terms of statistics for the total (global) image. For binary quantization, T was chosen as the median value in the larger image. This choice for T gives an equal number of plus and minus ones in the larger image. For the tri-level quantization, choosing T_1 as the lower 1/3 and T_2 as the 2/3 level in terms of total pixels in the amplitude histogram (ie 33 and 67 percentiles) gives an equal number of pixels at -1, 0 and +1 for the output quantized image. In summary the following thresholds were used.

$$\left.\begin{aligned} T &= \text{median} \quad \text{(binary)} \\ T_1 &= 33 \text{ percentile} \\ T_2 &= 67 \text{ percentile} \end{aligned}\right\} \text{(tri-level)}$$

Alternate choices were available and are included in the program software. These include

$$\left.\begin{aligned} T &= \mu \pm k\sigma \\ T_{1,2} &= \mu \pm k\sigma \\ T_{1,2} &= \text{low \%, high \%} \end{aligned}\right\} \qquad (4\text{-}1)$$

where μ is the mean, σ is standard deviation and k is a specifiable constant.

4.2 Adaptive Binary Quantizer. A locally adaptive binary quantizer was implemented which results in a quantized image that retains the image high frequency content. The center pixel in a 3 x 3 array is quantized dependent on a statistical threshold calculated within that window. As the window moves across the image the threshold is modified and used to quantize the middle pixel in the window.

Specifically,

T = median in a 3 x 3 window.

This adaptive method retains the image high frequency content and should result in a sharper correlation peak for the DCC or MAD algorithms. Further it has the advantage of relatively simple implementation in real time, especially if the mean instead of the median is used as the threshold. Simulation results in section 5 will compare correlation sharpness for the global and locally adaptive quantizers.

4.3 Gradient Processing. Gradient preprocessing of the images prior to correlation offers two potential advantages. First the gradient operation enhances high frequency content and should result in a sharper correlation peak. Secondly, gradient processing emphasizes edge features in an image, which may be the only features of similarity among different spectral band images of a given scene.

There are numerous gradient processors from which to choose including the Roberts cross operator, Laplacian and convolutional windows of varying geometries and coefficient values. Because of its simplicity a Prewitt magnitude gradient operation was applied to the images prior to quantization and/or correlation. The gradient is calculated from

$$g(m,n) = \left|g_1(m,n)\right| + \left|g_2(m,n)\right| \qquad (4-1)$$

where $g_1(m,n)$ results from convolving images r and s with window w_1 and $g_2(m,n)$ results from convolution with window w_2. These windows were

$$w_1 = \begin{bmatrix} -1 & -1 & -1 \\ 0 & 0 & 0 \\ 1 & 1 & 1 \end{bmatrix} \qquad w_2 = \begin{bmatrix} -1 & 0 & 1 \\ -1 & 0 & 1 \\ -1 & 0 & 1 \end{bmatrix} \qquad (4\text{-}3)$$

4.4 Gain and Mean Correction. The thresholded difference method is especially sensitive to errors in mean value or gain between two images to be correlated. This was illustrated in Figure 2.1 d) e) and f) where it is clear that these errors (even at registration) shift values off the r=s line in the joint pdf domain. Both these problems are eliminated if r and s images are first scaled to the same amplitude range, provided that neither image function is clipped. Consider a function, r, which is linearly represented over the range r_{min} to r_{max} and a function, s, which is linearly represented over the range s_{min} to s_{max} as shown in Figure 4.2.

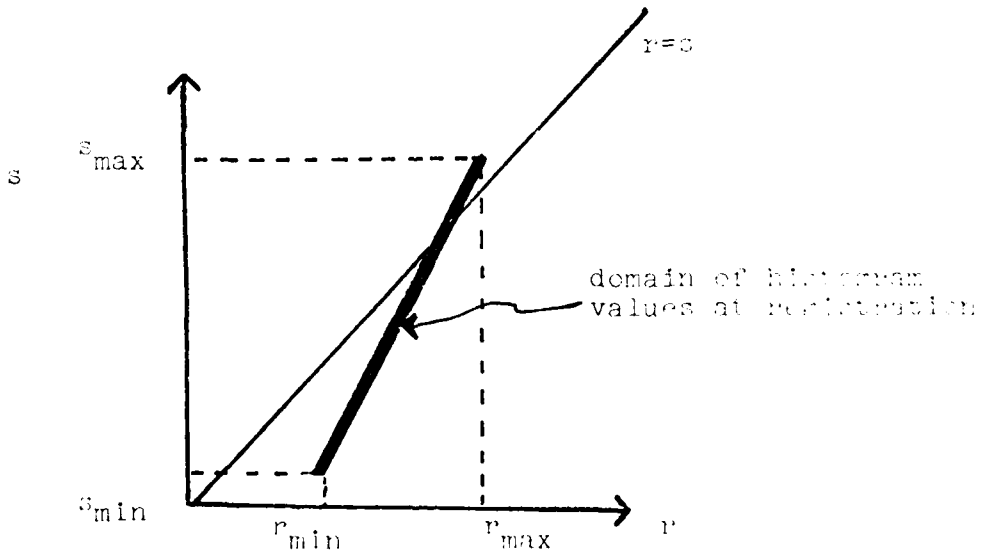

Figure 4.2 Gain and Mean Errors in Joint Histogram Domain

The domain of histogram values at registration, i.e. on the dark line in Figure 4.., is mapped onto the r=s line by a simple linear rescaling of r and s which maps

$$r_{min} \longrightarrow 0 \qquad s_{min} \longrightarrow 0$$
$$r_{max} \longrightarrow 255 \qquad s_{max} \longrightarrow 255 \tag{4-4}$$

This rescaling was applied as a necessary pre-processing step prior to the thresholded difference correlation algorithm. The rescaling is accomplished using equations (4-5) and (4-6).

$$r(\text{re-scaled}) = \frac{r-r_{min}}{r_{max}-r_{min}} \cdot 255 \tag{4-5}$$

$$s(\text{re-scaled}) = \frac{s-s_{min}}{s_{max}-s_{min}} \cdot 255 \tag{4-6}$$

For the case of uncorrelated noise in r and s, the linear re-scaling applied to signal plus noise will force pixels that are matched to lie off the r=s line. For the thresholded difference method to work in this case requires that the threshold be increased to allow larger differences between r and s. Further the threshold should be related to the rms noise levels in the two images.

5. SIMULATION RESULTS

All algorithms were first tested using simple input arrays of data for which the processing results were predictable. Next the various registration metrics were applied to actual electro-optical imagery. The results of those simulations are described in this section. A summary of the simulations done is given in Figure 5.1. Over 120 simulation runs

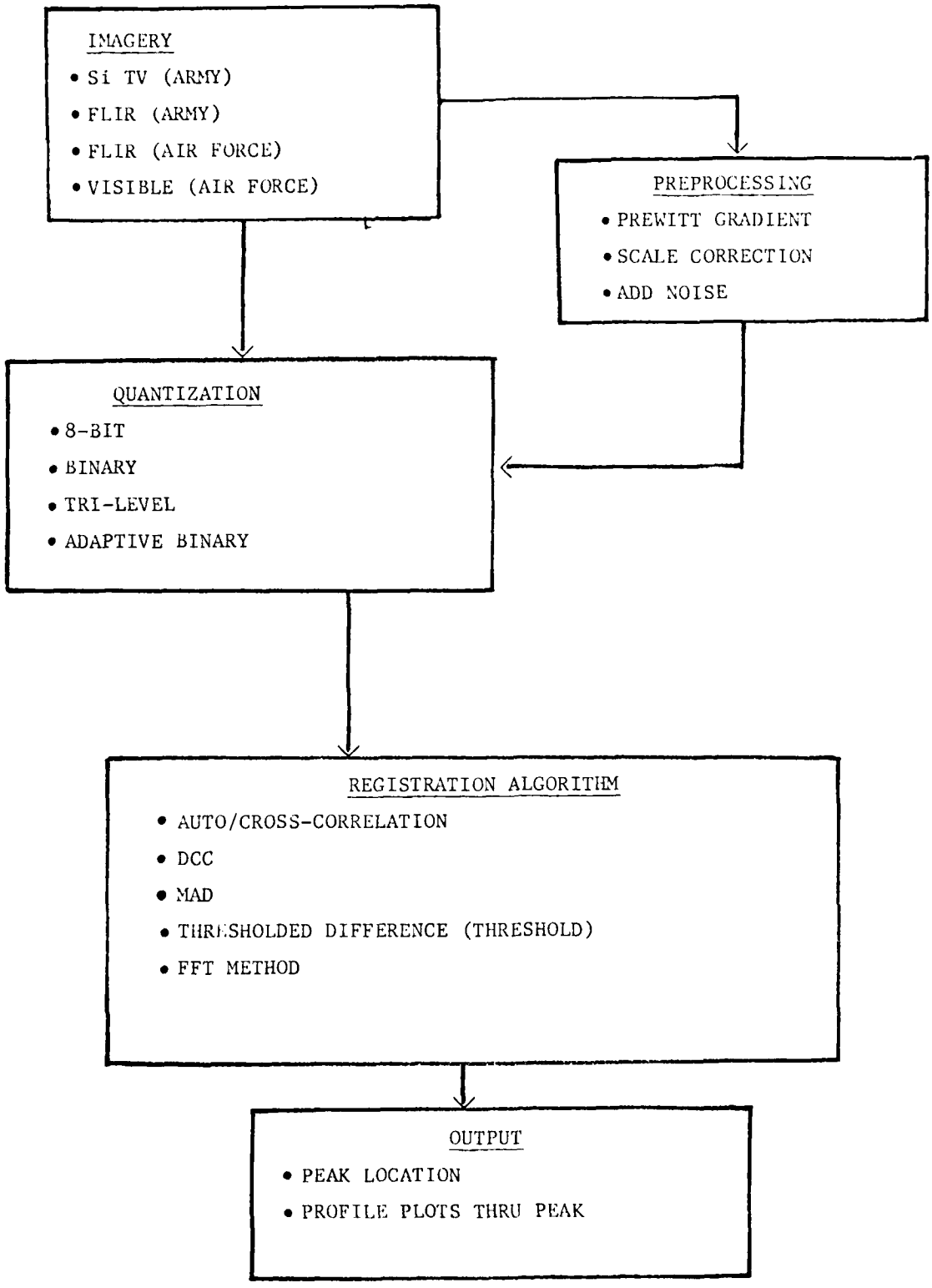

Figure 5.1 Simulation Options Summary

were made which compare the direct cross correlation, mean absolute difference and thresholded difference registration metrics. The effects of noise, scene content, time of day variations, different spectral bands and different scale are illustrated by the simulations. Further, the effects of binary, tri-level and 8-bit quantization as well as gradient pre-processing and an adaptive binary quantizer are shown by selected simulations.

5.1 Scene Descriptions. Imagery for use in the correlator simulations was obtained from two sources:

1. the U. S. Army Missile Command, Redstone Arsenal, Alabama; and
2. the U.S. Air Force through The Analytic Sciences Corporation (TASC).

Both data sets contain multi-spectral, low altitude, short range imagery from co-located sensors.

Ten image files were established from the data tapes for input to the simulation program. A brief description of these images is given in Table 5.1.

The first four images were used in auto-correlation calculations to provide a known registration point for comparing algorithms and quantization methods. To accomplish this, reference and sensed images were established as shown in Figure 5.2. The reference image is extracted as the 64 x 64 center portion of the larger 128 x 128 sensed image.

TABLE 5.1 Scene Descriptions

DESIGNATION	SPECTRAL BAND	DESCRIPTION	SIZE (PIXELS)	COMMENTS
1. SCENE 1	Si TV	TARGET/TREE-FIELD BKGD.	407	CONTROL IMAGES
2. SCENE 2	Si TV	TARGET/FIELD BKGD.		FOR
3. SCENE 3	Si TV	GRADIENT OF SCENE 1	BY	ALGORITHM
4. SCENE 4	Si TV	GRADIENT OF SCENE 2	392	COMPARISON
5. OHIO FILE 2	8-12μ	BUILDING COMPLEX (25) (NOON)	150	SAME SCENE
6. OHIO FILE 10	8-12μ	BUILDING COMPLEX (25) (2:00 PM)	BY 150	DIFFERENT TIME-OF-DAY
7. OHIO FILE 26	8-12μ	BUILDING COMPLEX (26)	80	SAME SCENE
8. OHIO FILE 27	VISIBLE	BUILDING COMPLEX (26)	BY 128	DIFFERENT SPECTRAL BAND
9. HSV FILE	FLIR	NFOV WHITE HOT, TGT #3	407	SAME SCENE
10. HSV FILE	Si TV	WFOV TGT #3	BY 392	DIFFERENT SPECTRAL BAND
				DIFFERENT SCALE, CONTRAST REVERSED

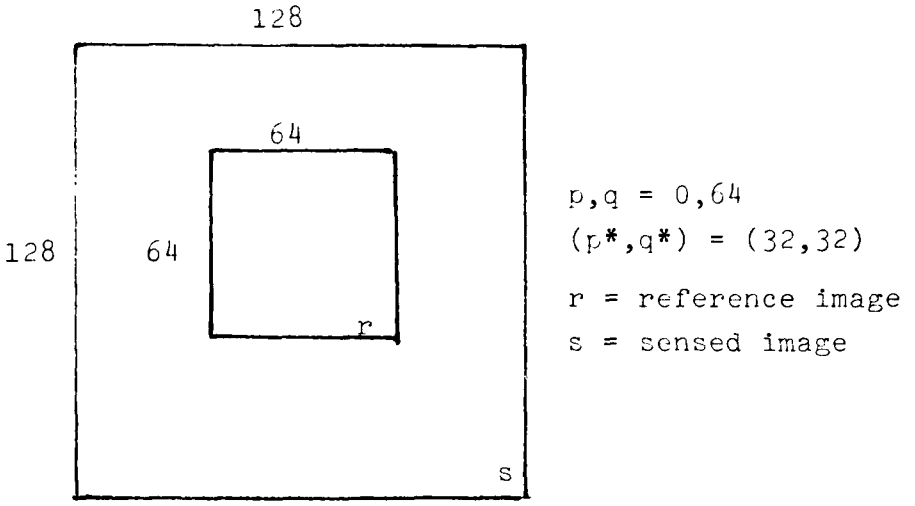

Figure 5.2 Image Segments from Silicon TV

Registration then occurs at a shift position (p*,q*) = (32,32).

For Ohio Files 2 and 10 the geometry shown in Figure 5.3 was used. The reference image was selected as the central 50 by 50 pixels from File 2. This image was then correlated with the larger 150 by 150 sensed image (File 10).

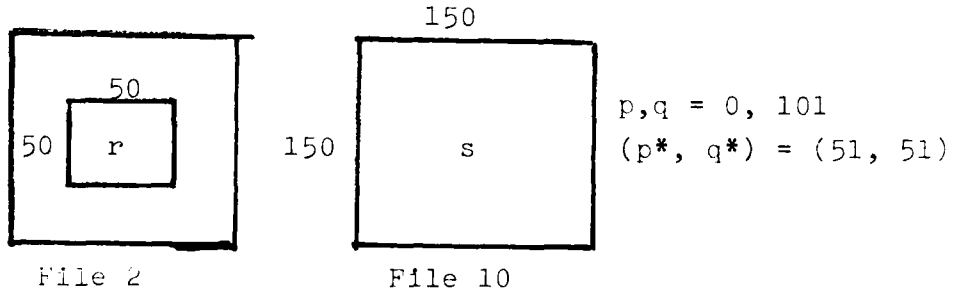

Figure 5.3 Ohio Files 2 and 10 Image Segments

For Ohio Files 26 and 27 the image geometries shown in Figure 5.4 was used. The reference image was taken as the lower right quadrant of file 26 (40 x 64 pixels). This segment was correlated with the entire (80 x 128 pixels) File 27 image.

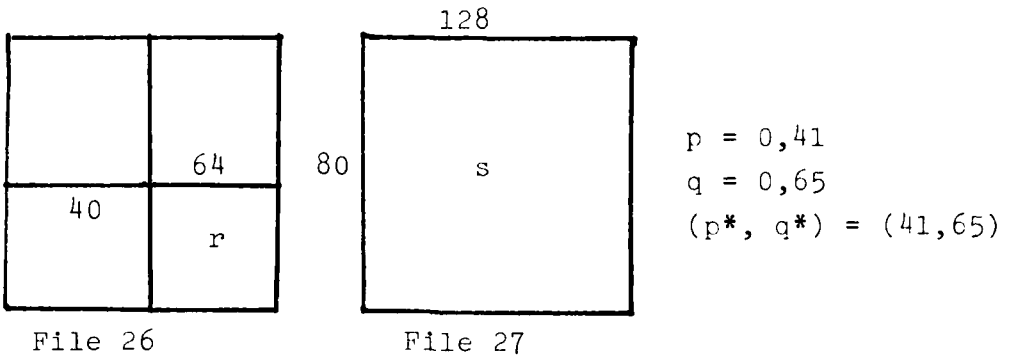

Figure 5.4 Ohio Files 26 and 27 Image Segments

For the HSV Files 9 and 10, there was a difference in scale as well as spectral band. An area of commonality was selected visually from photographs. Scale difference was computed from dimensions of a large rectangular target board in the two images. Since File 10 was a narrow field-of-view (NFOV) image, objects in File 10 appeared larger than in File 9 by a ratio determined to be 1.0/0.55. Scaling was applied to reduce the size of objects in File 10 to match the smaller size in File 9. After scaling, File 10 then had only 233 by 215 pixels. Figure 5.5 shows the relative geometries for image segments from HSV Files 9 and 10. A 56 x 75 reference

image is obtained

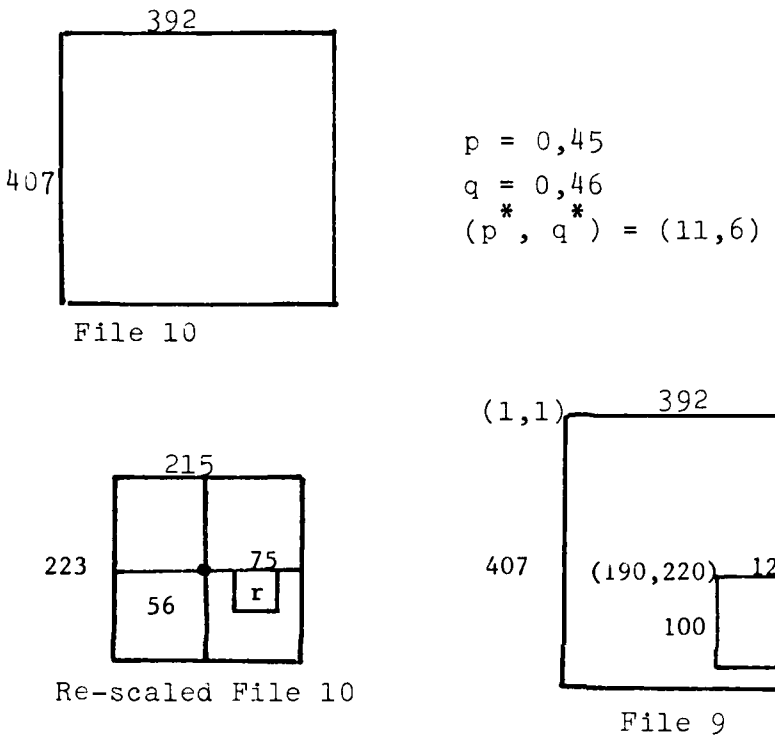

Figure 5.5 HSV Files 9 & 10 Image Segments

from File 10 and a 100 x 120 sensed image is obtained from File 9 with a match at shift $(p^*, q^*) = (11,6)$.

5.2 Metric Comparison. Comparison of the direct cross correlation (DCC), mean absolute difference (MAD) and thresholded difference (TD) metrics is given in this section for the noise-free correlation of imagery represented by Scene 1 and Scene 2 (ie autocorrelation of Silicon TV imagery) as shown in Figure 5.2. Results are shown for 8-bit, binary and tri-level quantizations.

Results are shown in Figures 5.6 thru 5.9 for Scene 1 and in Figures 5.10 thru 5.13 for Scene 2. The figures show cross-sectional plots through the correlation peak in vertical and horizontal directions respectively. Peak sharpness is greater in the vertical direction for both images. This was felt to be a result of the limited sampling rate applied to the 875 line video from which the images were obtained. The expected result would be reduced frequency content (and a broader correlation peak) for the horizontal direction.

The comparisons shown in Figure 5.6 are a) 8-bit DCC (either direct or FFT implementation), b) 8-bit MAD, c) binary DCC or MAD, d) tri-level MAD and e) tri-level DCC. All methods gave the correct peak location of 32 and peak amplitudes as expected from algorithm definitions for ideal registration. Thus the only feature for comparison is relative peak sharpness. As can be seen, there are only slight variations in peak sharpness among the five methods in Figure 5.6.

In Figure 5.7, a) 8-bit DCC repeated for comparison, b) TD (T=0), c) TD (T=2), d) TD (T=5) and e) TD (T=10) simulations are shown for the same conditions as Figure 5.6. The thresholded difference method is clearly superior in terms of correlation peak sharpness if the threshold, T, can be kept small. It should be emphasized here that a threshold of T=0 gives almost perfect results for the ideal conditions under which the correlation was done (ie at registration the images were known to be a perfect match). For cross-correlation

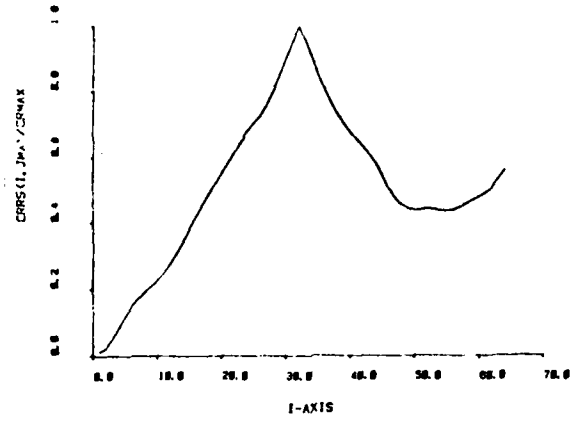

a) DCC 8-bit

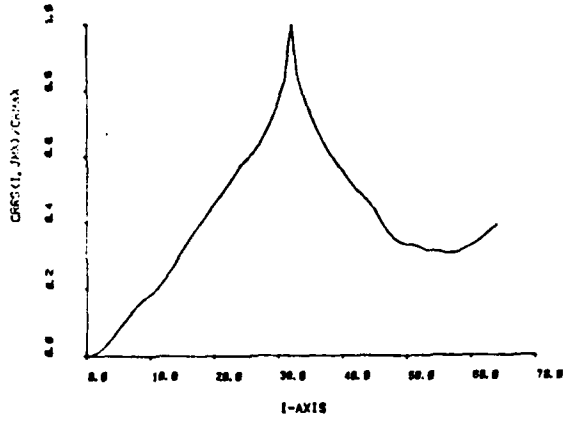

b) MAD 8-bit

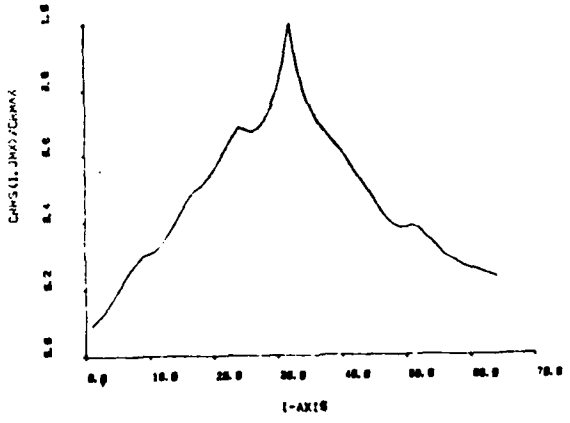

c) BINARY DCC or MAD

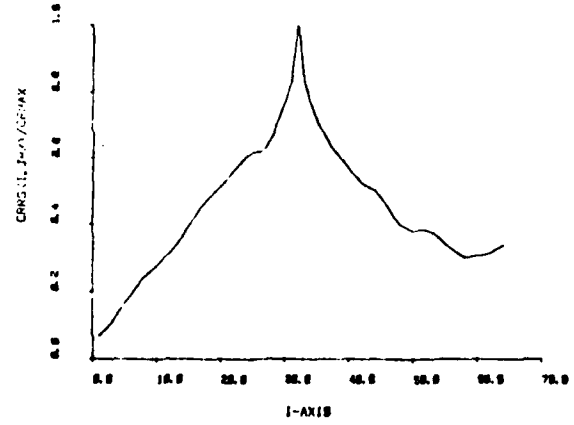

d) TRI-LEVEL MAD

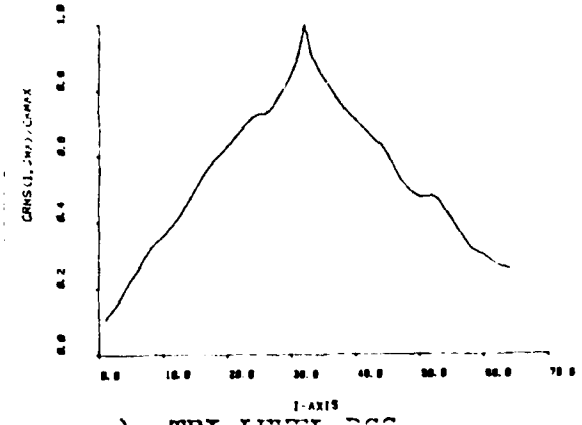

e) TRI-LEVEL DCC

Figure 5.6 Scene 1, Vertical Profiles Through Peak (Noise-free)

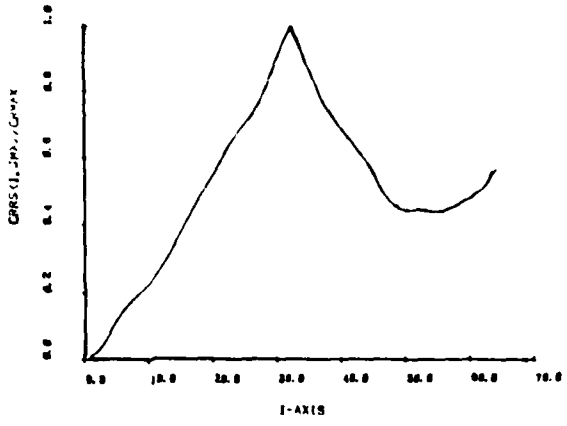

a) DCC 8-bit

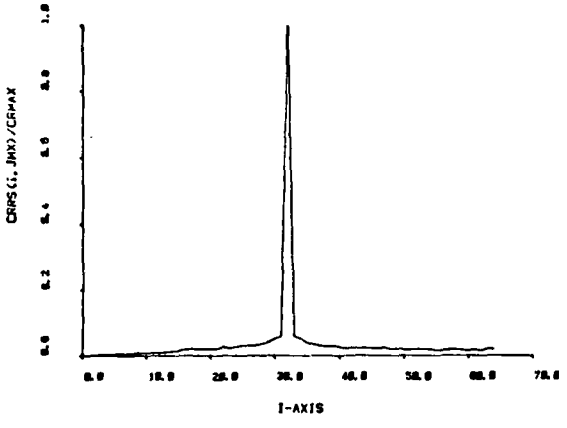

b) TD (T=0)

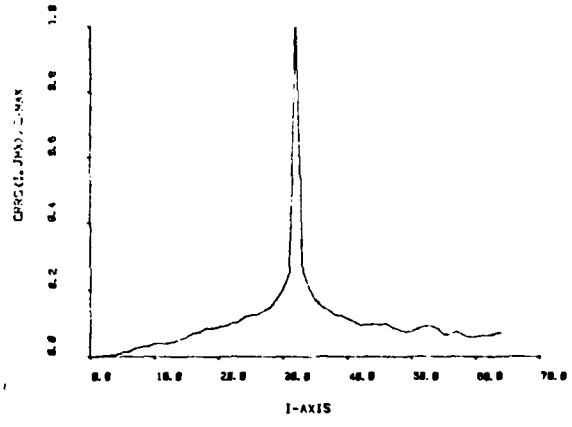

c) TD (T=2)

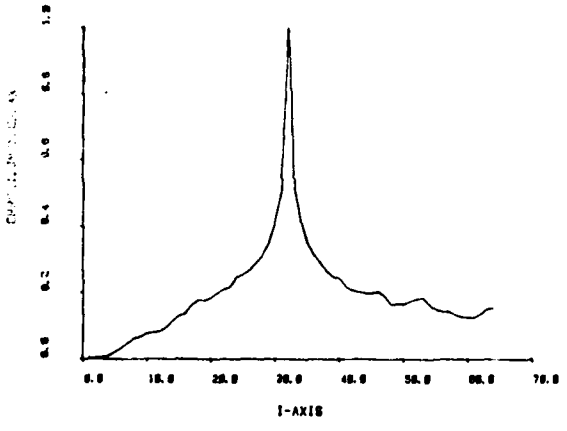

d) TD (T=5)

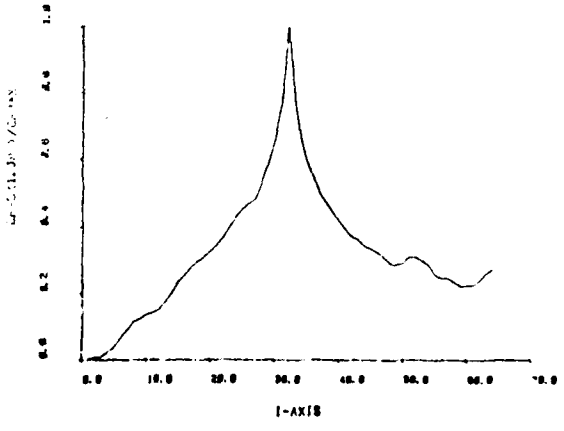

e) TD (T=10)

Figure 5.7 Thresholded Difference, Scene 1, Vertical (Noise Free)

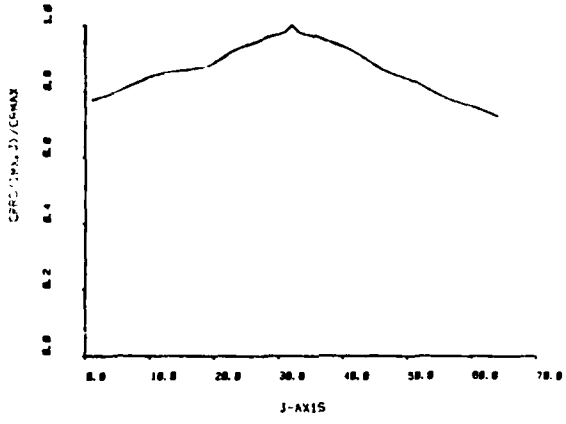

a) DCC 8-bit

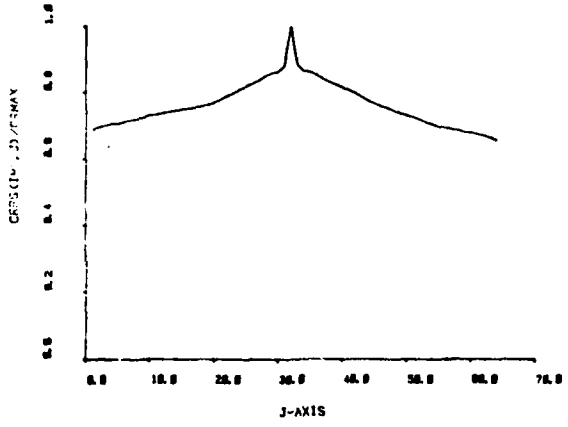

b) MAD 8-bit

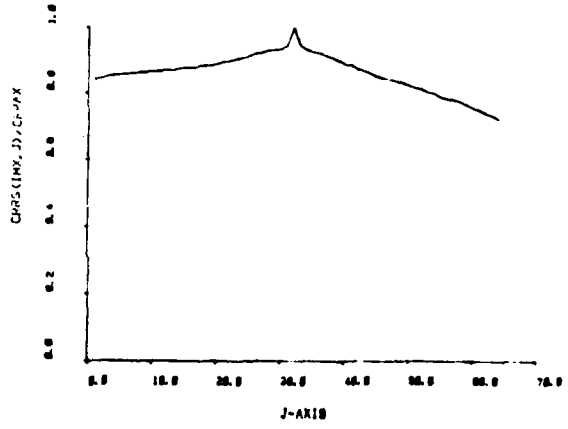

c) BINARY DCC or MAD

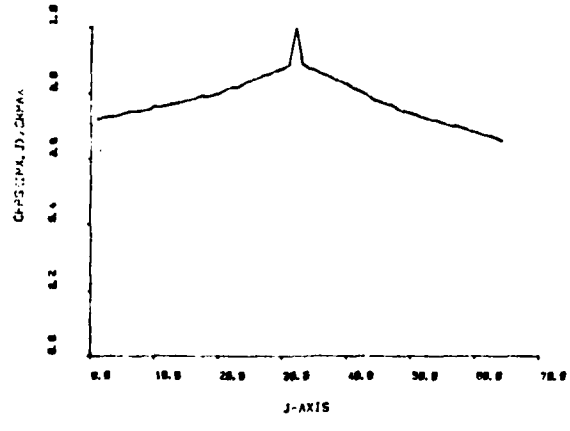

d) TRI-LEVEL MAD

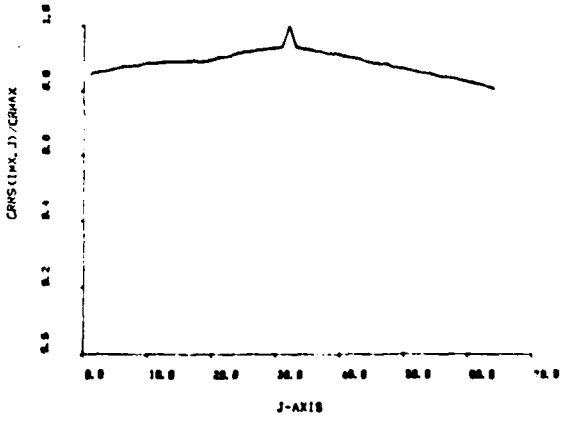

e) TRI-LEVEL DCC

Figure 5.8 Scene 1, Horizontal Profiles Through Peak (Noise-free)

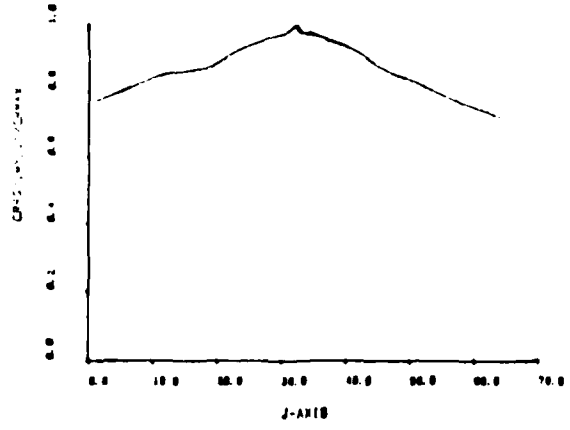

a) [illegible] 8-bit

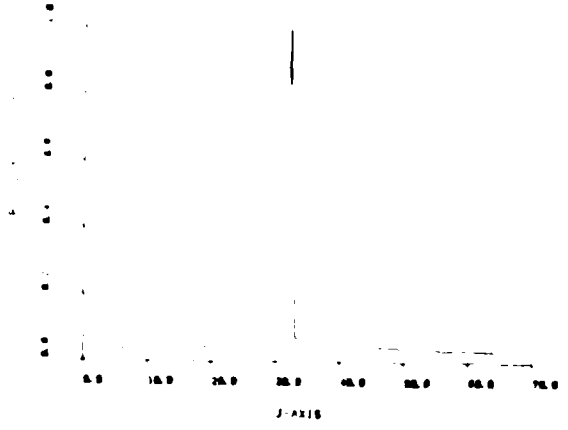

b) [illegible]

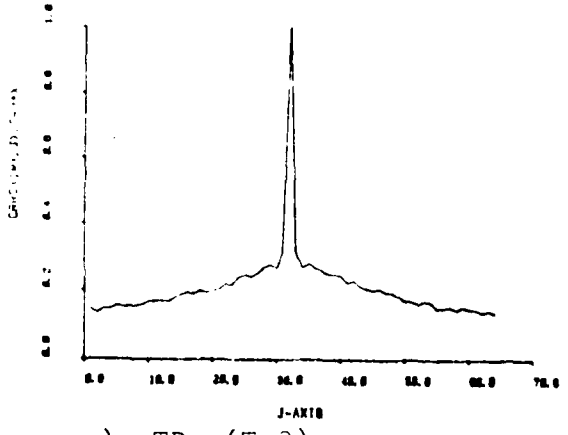

c) TD (T=2)

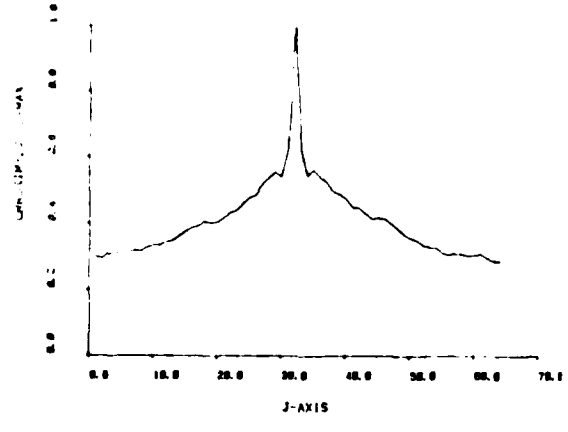

d) TD (T=5)

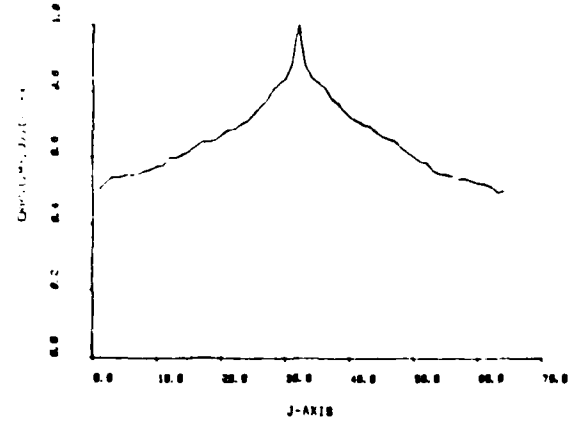

e) TD (T=10)

Figure 5.9 Thresholded Difference, Scene 1, Horizontal (Noise-free)

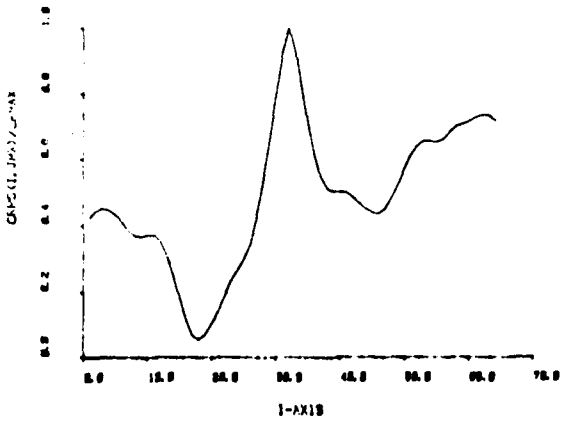

a) DCC 8-bit

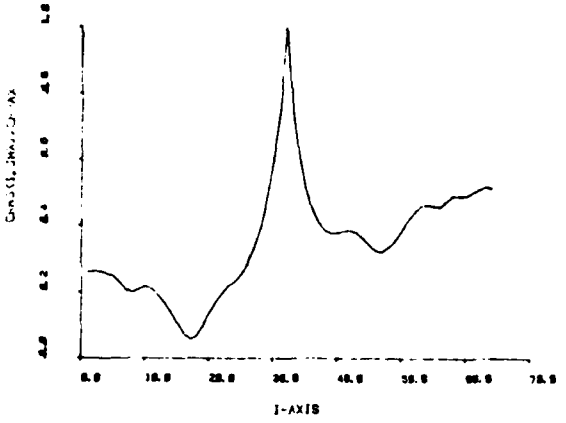

b) MAD 8-bit

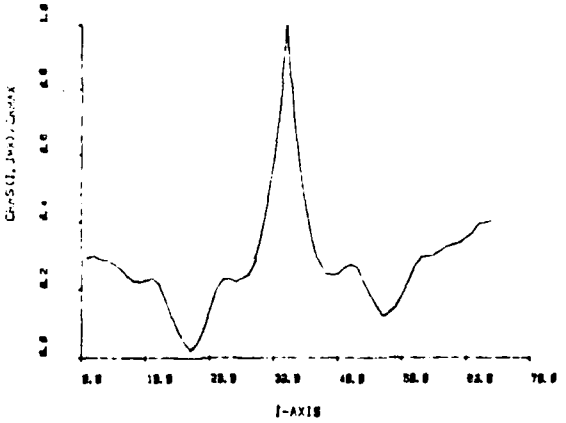

c) BINARY DCC or MAD

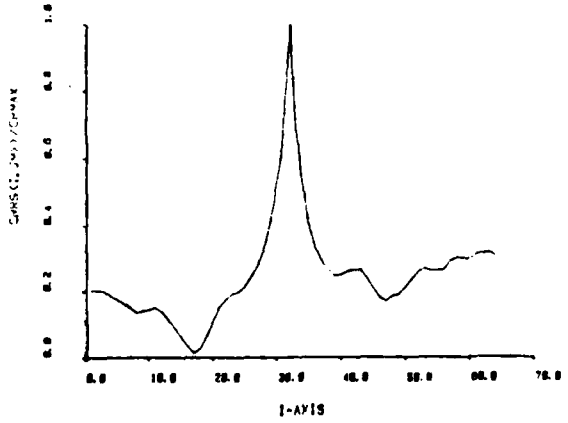

d) TRI-LEVEL MAD

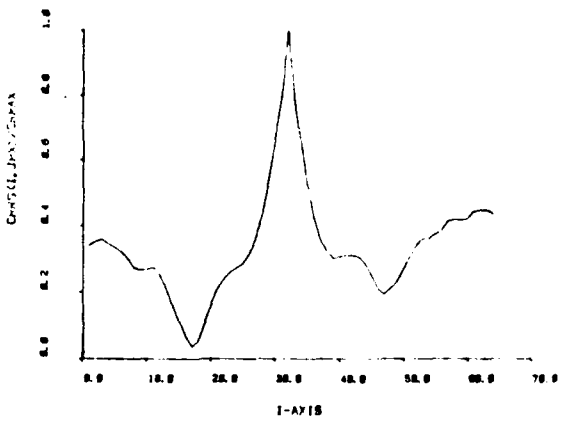

e) TRI-LEVEL DCC

Figure 5.10 Scene 2, Vertical Profiles Through Peak (Noise-free)

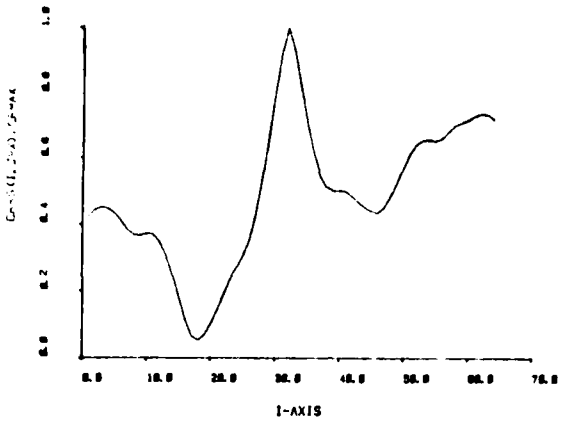

a) DCC 8-bit

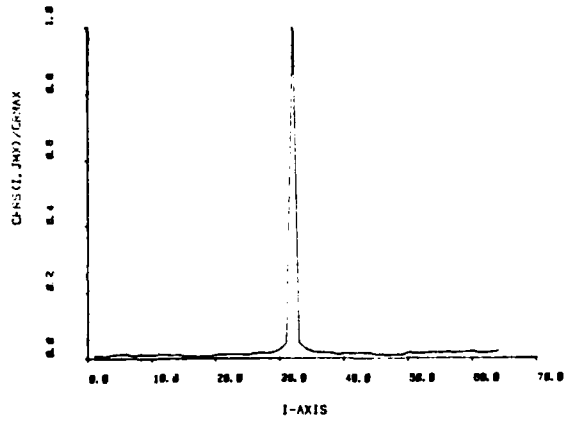

b) TD (T=0)

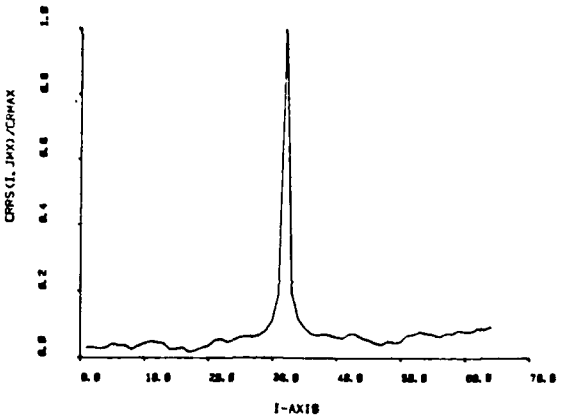

c) TD (T=2)

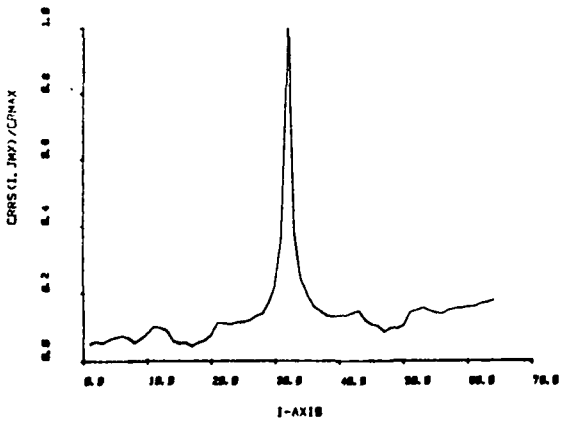

d) TD (T=5)

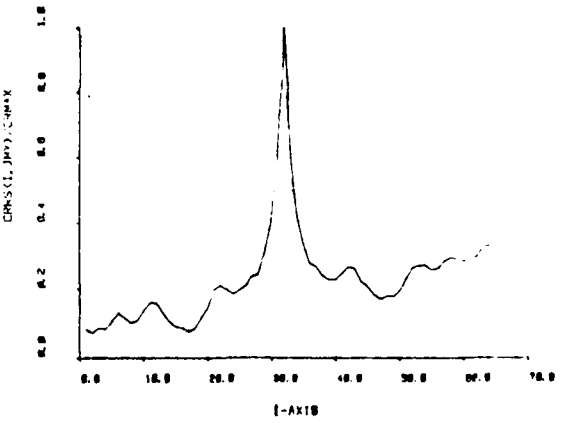

e) TD (T=10)

Figure 5.11 Thresholded Difference, Scene 2, Vertical (Noise-free)

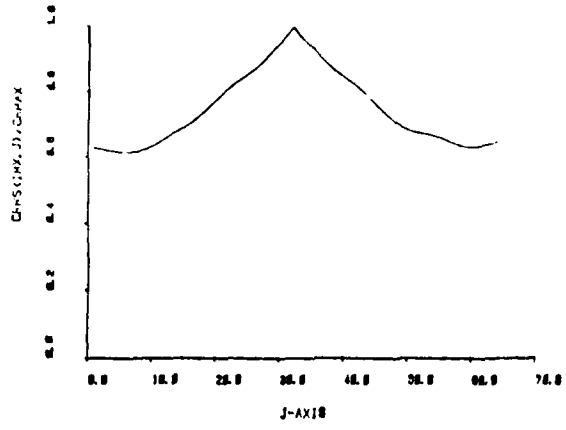

a) DCC 8-bit

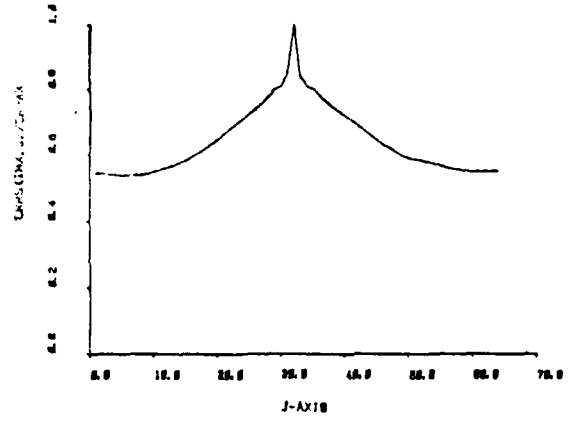

b) MAD 8-bit

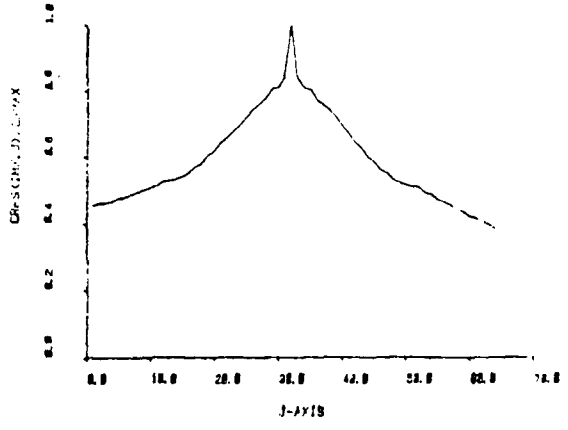

c) BINARY DCC or MAD

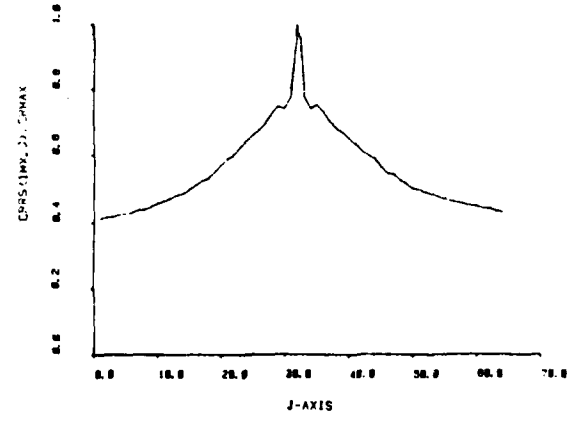

d) TRI-LEVEL MAD

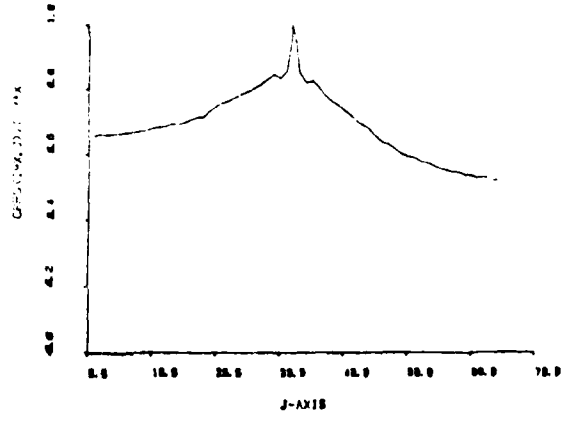

e) TRI-LEVEL DCC

Figure 5.12 Scene 2, Horizontal Profiles Through Peak (Noise-free)

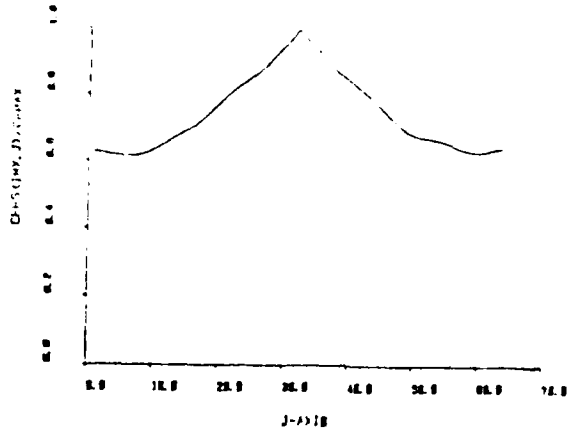

a) DCC 8-bit

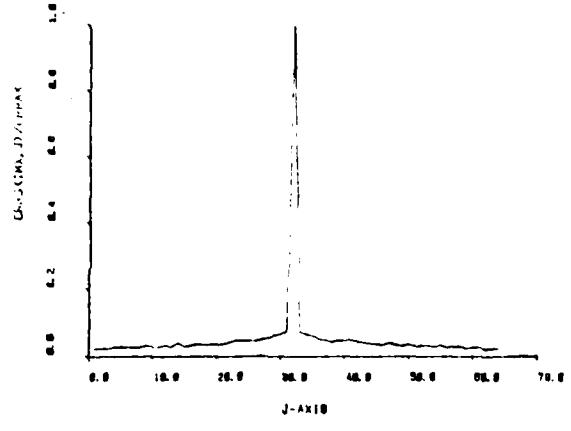

b) TD (T=)

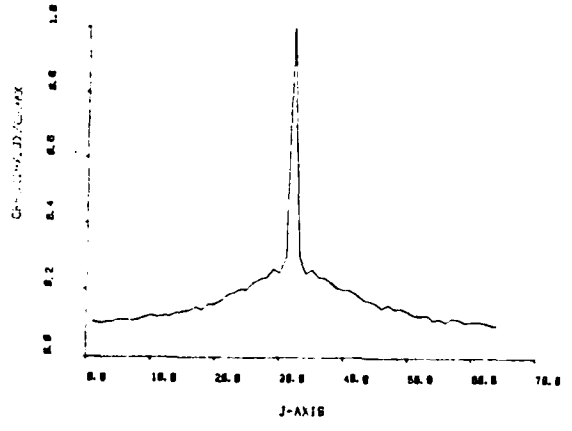

c) TD (T=2)

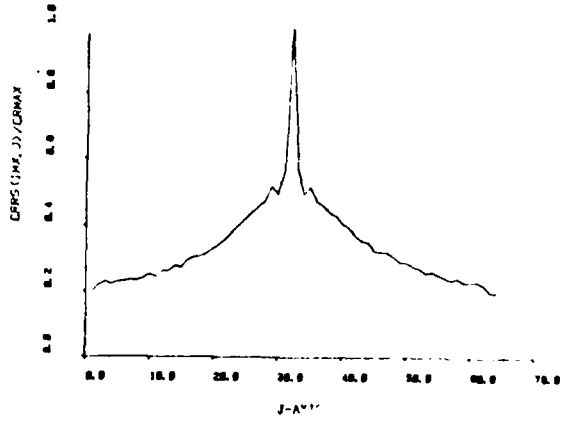

d) TD (T=5)

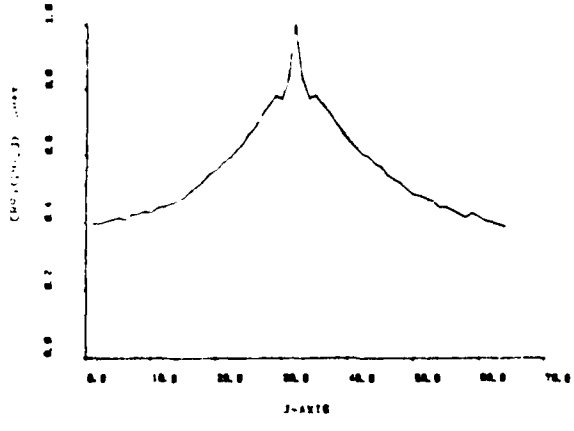

e) TD (T=10)

Figure 5.13 Thresholded Difference, Scene 2, Horizontal (Noise-free)

of realistic images it is likely that a number of pixels will vary in amplitude between the two images at registration. Exactly how much they vary would depend on signal-to-noise ratios, geometric distortion and sensor anomalies.

In comparing the threshold values shown in the figure, one should evaluate T as the allowable error between two gray levels which each have a possible range of 8 bits (0-255).

A comparison which illustrates that the TD method is a high frequency emphasis method is shown in Figure 5.8 and 5.9 for the peak profile in the horizontal direction for Scene 1. A very flat correlation peak (easily obscured by noise) is produced by all methods except the TD method which produces a peak whose sharpness again depends on the value of T. If the images are known to be of high quality (low noise, low distortion) then it is possible to achieve high correlation accuracy with the TD method (using a low value of T), even if the scene has low frequencies only.

Additional comparisons are provided by Figures 5.10 through 5.13 which give peak profiles in vertical and horizontal directions for Scene 2.

5.3 Noise Effects on Registration Peak. To evaluate the effects of uncorrelated noise on the different registration metrics, random noise was added to r and s on a pixel by pixel basis and independently for each image. Noise-free r and s images were taken from Scene 1 as indicated in Figure 5.2.

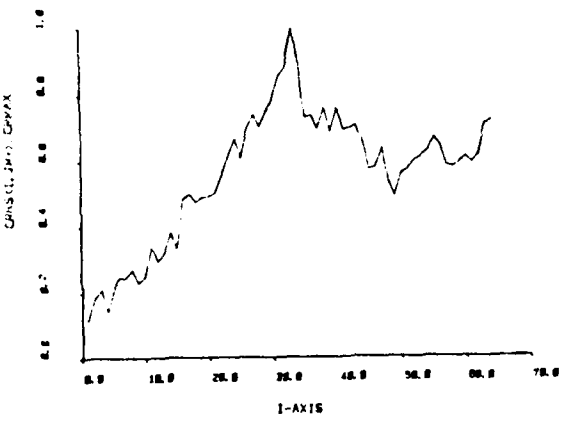

a) DCC 8-bit

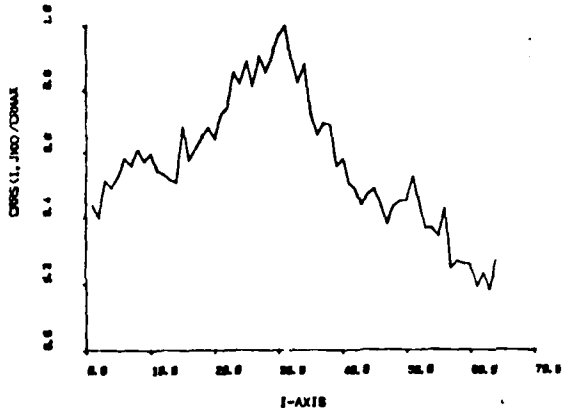

b) BINARY DCC or MAD

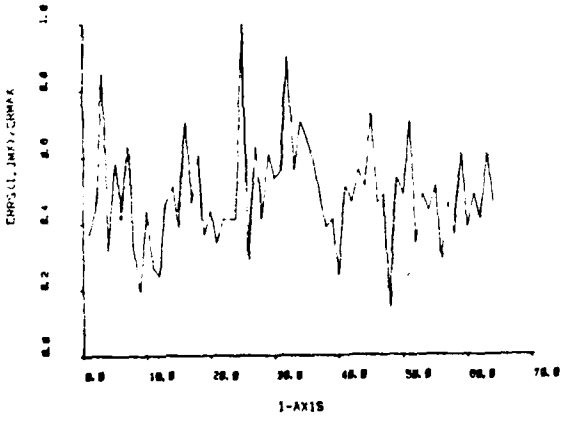

c) TD (T=0)

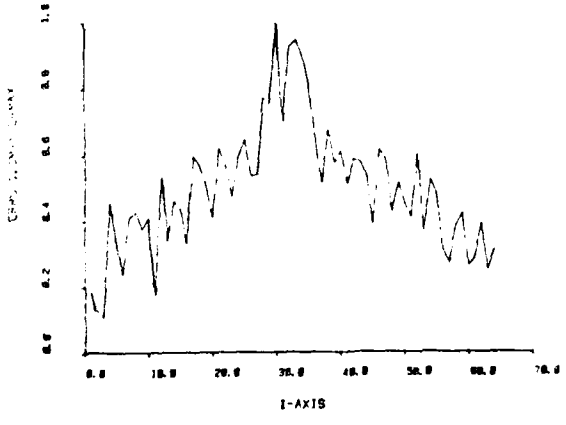

d) TD (T=20)

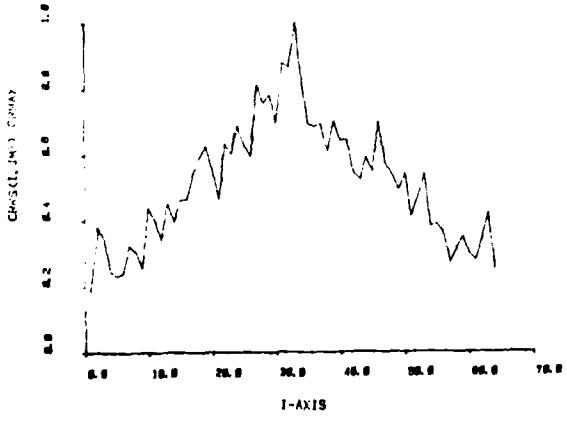

e) TD (T=40)

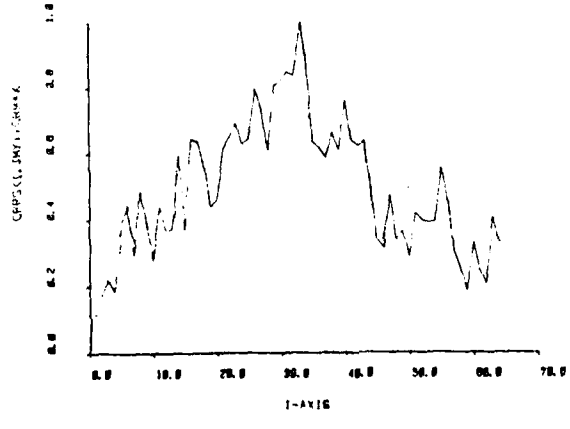

f) TD (T=100)

Figure 5.14 Scene 1, Additive Noise (S/N = 0.43) (Vertical)

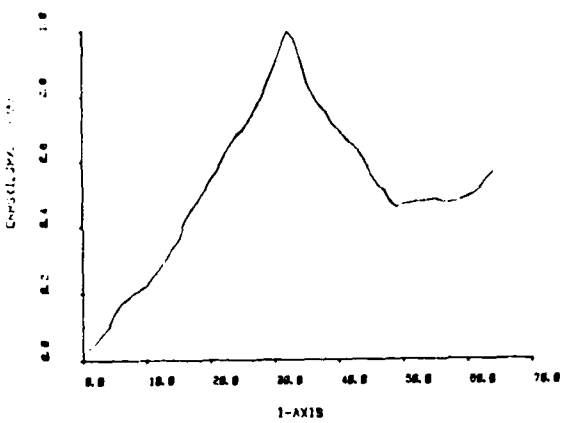

a) DCC 8-bit

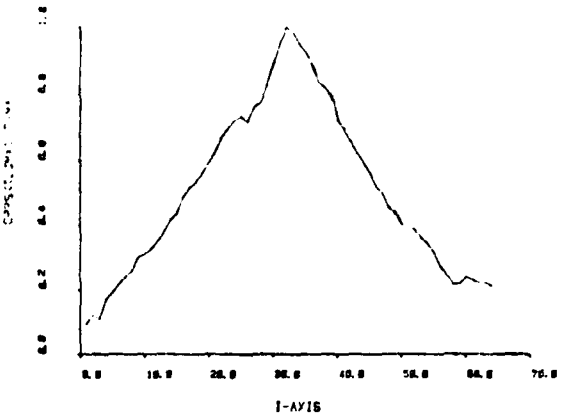

b) BINARY DCC or MAD

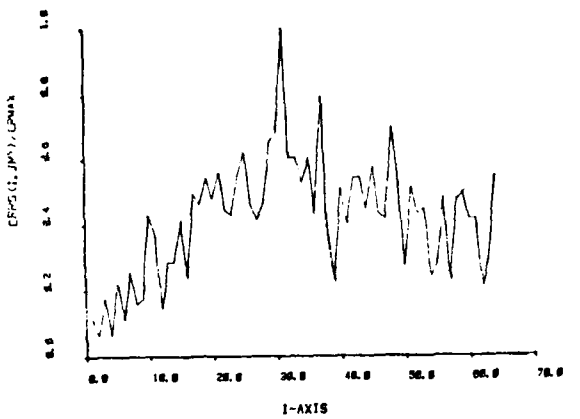

c) TD (T=0)

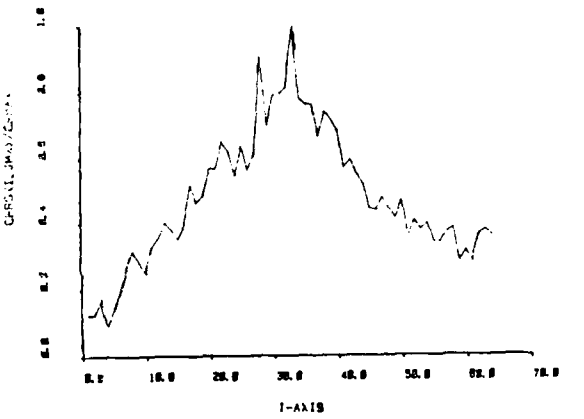

d) TD (T=2)

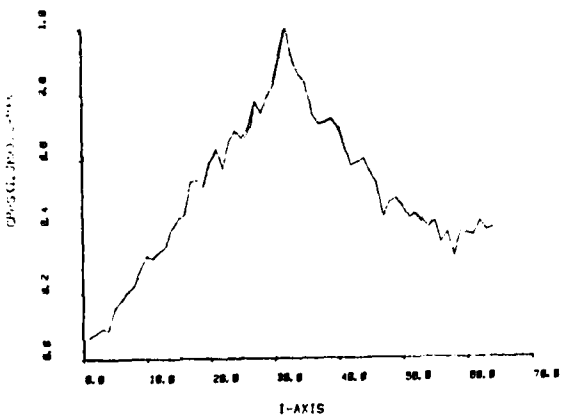

e) TD (T=10)

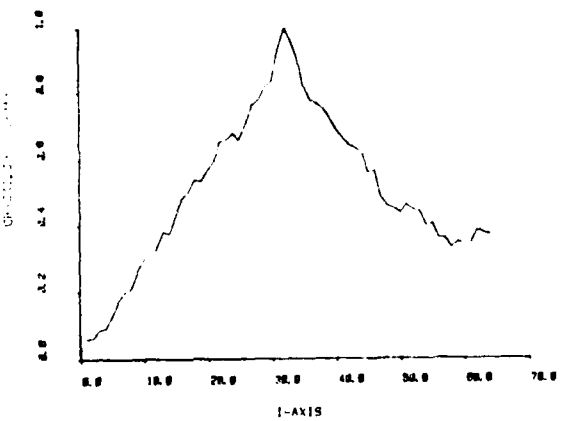

f) TD (T=30)

Figure 5.15 Scene 1, Additive Noise (S/N = 1.42) (Vertical)

Zero-mean random noise with specifiable standard deviation was added to each image prior to quantization and correlation.

Two sets of simulations were done representing fairly high noise levels. Signal-to-noise ratios were defined as

$$SNR = \frac{\sigma}{\sigma_n} \tag{5-1}$$

where σ is the image standard deviation (image r or s) and σ_n is the specifiable noise standard deviation. For one set of simulations a SNR of 0.43 was used, and for the other set, a SNR of 1.42 was used. Example results are given as vertical profiles through the peak in Figure 5.14 for SNR = 0.43 and Figure 5.15 for SNR = 1.42. Each figure compares a) 8-bit DCC, b) binary DCC or MAD and c), d), e), f) TD for four different thresholds.

It is clear that the TD method (which is a high frequency emphasis method) is more sensitive to the high frequency (pixel by pixel) noise added to the images. It even produces false peaks for very low values of T. Performance of the TD method is similar to the DCC method if T is "large enough". The value of T which is "large enough" depends on noise level. For the two simulations, the TD method began to behave reasonably well at a threshold of $T = 0.5\ \sigma_n$. This is illustrated in Figure 5.14 e) where $T = 40 = .6\ \sigma_n$ (σ_n=65) and in Figure 5.15 e) where $T = 10 = 0.51\ \sigma_n$ ($\sigma_n = 19.5$).

Additional noise dependence is indicated in Table 5.2 which gives calculated peak locations for all the algorithms

tested for Scene 1 and SNR = 0.43 and 1.42. Note that errors are larger for the horizontal (second) peak location. This is expected since high frequency noise was added to an image with inherent low frequency in the horizontal direction.

TABLE 5.2 NOISE EFFECTS

Correct Peak Location (32,32)		
METHOD	COMPUTED PEAK LOCATION	
	SNR=0.43	SNR=1.42
DCC(8-Bit)	(33,32)	(32.32)
DCC(Tri-Level	(31,59)	(32.37)
DCC(Binary)	(31,59)	(32,32)
MAD(8-Bit)	(33,32)	(32.32)
MAD(Tri-Level	(31,59)	(33,32)
MAD(Binary)	(31,59)	(32,32)
TD (T=0)	(25,51)	(31,26)
TD (T=2)	X	(33,38)
TD (T=5)	X	(32,35)
TD (T=10)	X	(32,32)
TD (T=20)	(30,35)	(32,32)
TD (T=30)	X	(32,32)
TD (T=40)	(33,32)	X
TD (T=60)	(31,40)	X
TD (T=80)	(33,41)	X
TD (T=100)	(33,32)	X

5.4 Gradient Preprocessed Images. Gradient preprocessing by application of a 3 x 3 Prewitt operator to Scenes 1 and 2 was done prior to quantization and correlation. The resultant high-frequency-emphasized images should exhibit sharper correlation peaks.

The results are shown as peak profiles in Figure 5.16 Scene 1, Vertical; Figure 5.17 Scene 1, Horizontal; Figure 5.18 Scene 2, Vertical and Figure 5.19 Scene 2, Horizontal for various registration metrics. Results without and with gradient preprocessing are shown side-by-side for easy comparison. In every case except for the TD method, gradient preprocessing did produce a sharper correlation peak. It is postulated that since the TD method exhibits high frequency emphasis characteristics itself, then high-frequency-emphasis filtering provided by the gradient processor offers no additional gain. This "independence" of the TD method to gradient processing was observed for all values of T used in the simulations.

5.5 Adaptive Quantizer. A locally adaptive threshold was used to quantize images to 1 bit (binary quantization) before correlation. The threshold was computed as either the mean or median in a 3 x 3 moving window. At each location the center pixel is quantized about the threshold computed for that location.

This adaptive threshold in effect emphasizes the image high frequency content and should result in a much sharper

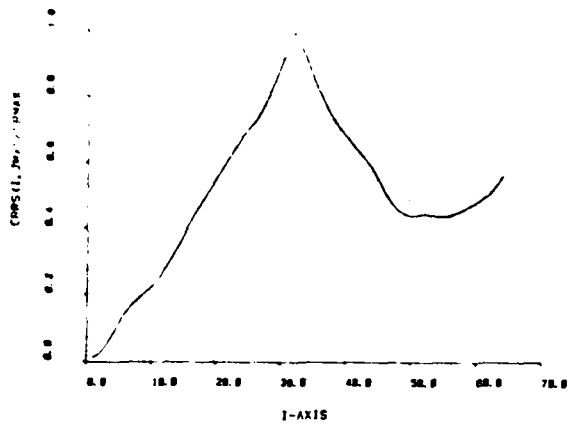

a) DCC 8-bit

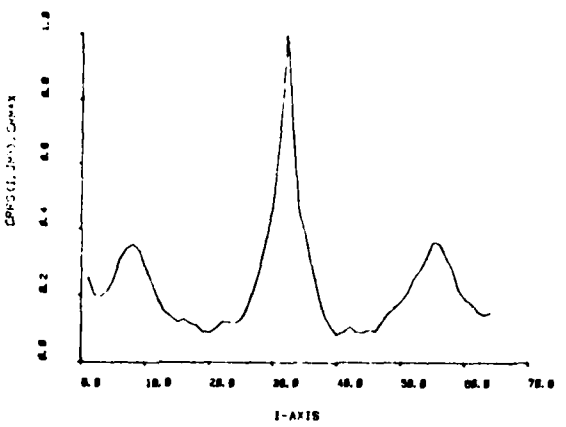

b) DCC 8-bit

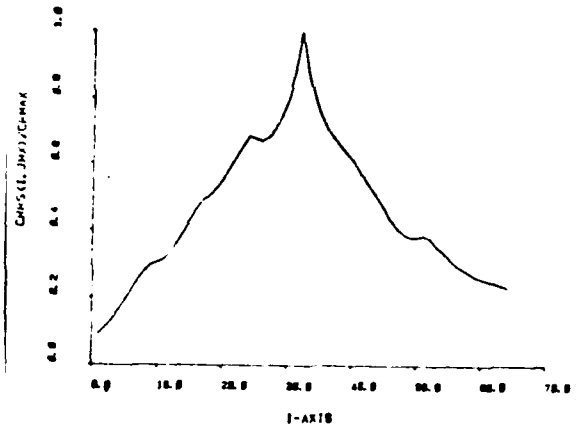

c) BINARY - DCC

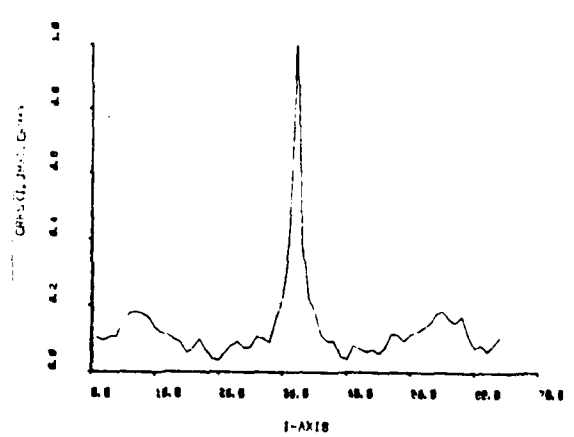

d) BINARY - DCC

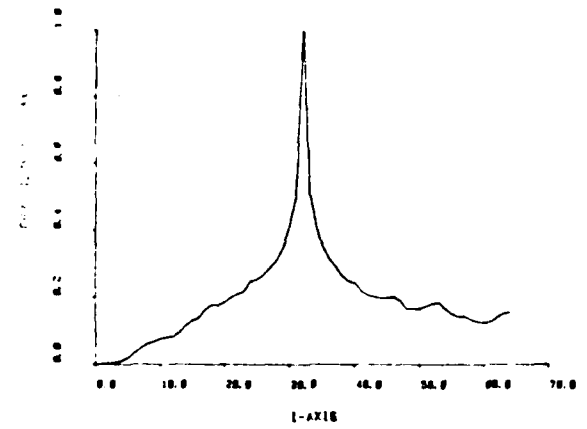

e) TD (T=5)

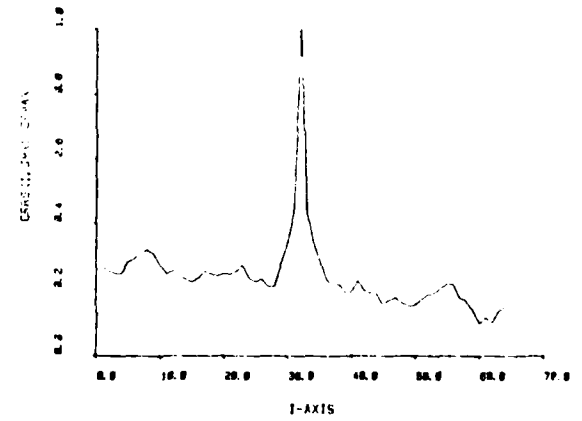

f) TD (T=5)

Figure 5.16 Scene 1, Vertical Profile, Gradient (Noise-free)

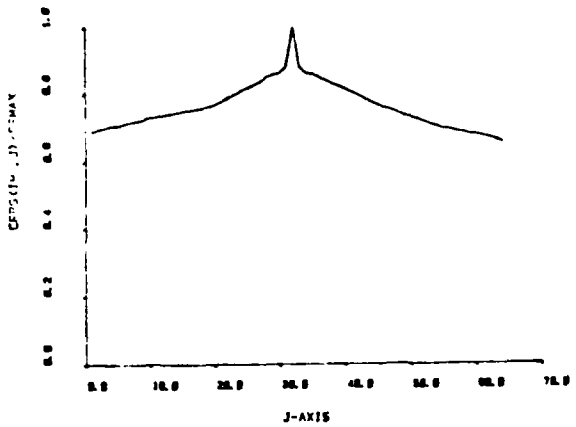

a) MAD 8-bit

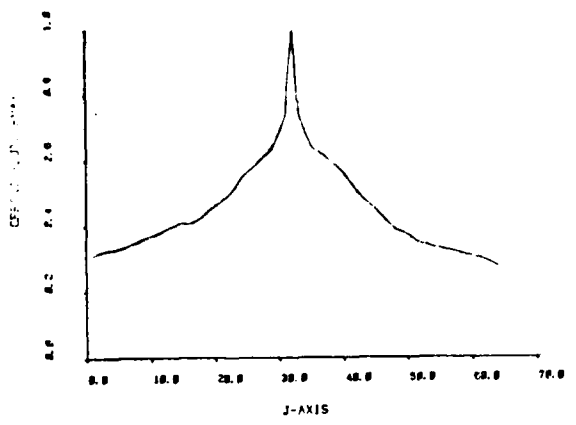

b) MAD 8-bit

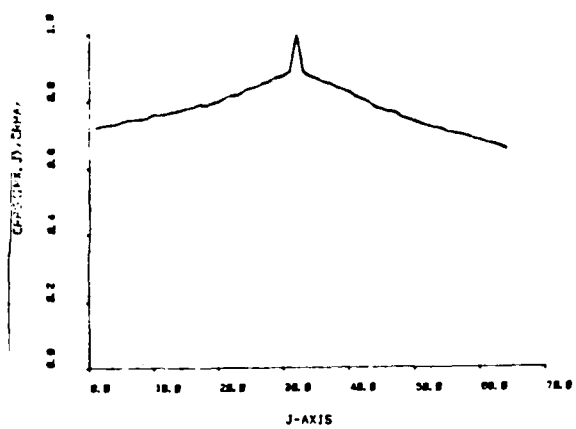

c) TRI-LEVEL - MAD

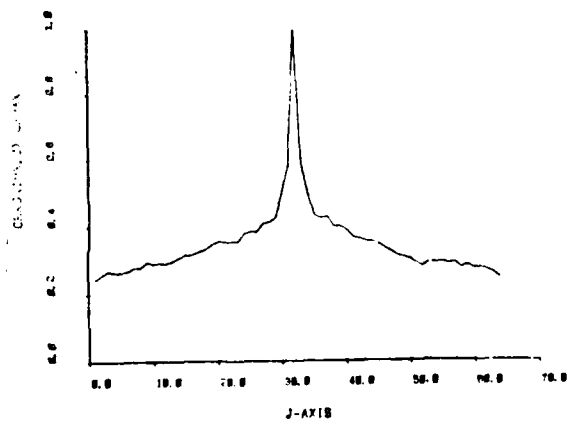

d) TRI-LEVEL - MAD

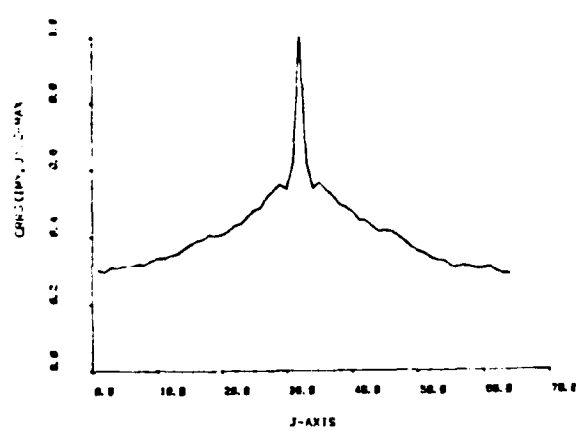

e) TD (T=5)

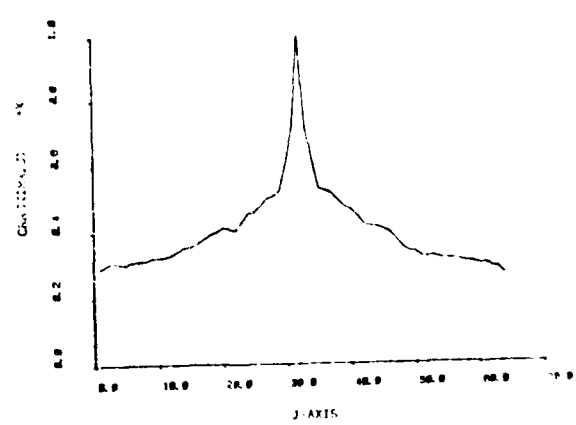

f) TD (T=5)

Figure 5.17 Scene 1, Horizontal Profile, Gradient (Noise-free)

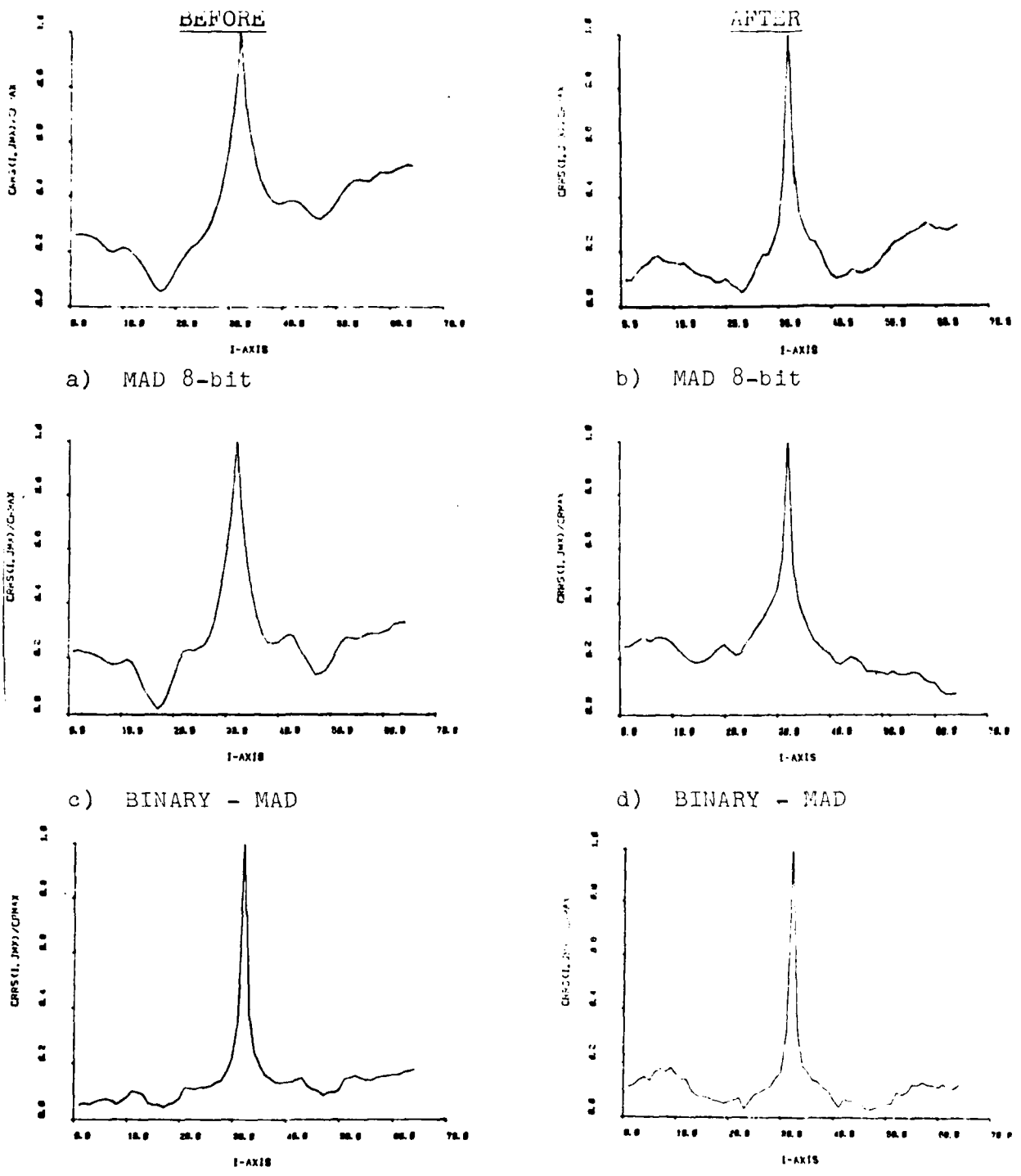

a) MAD 8-bit

b) MAD 8-bit

c) BINARY - MAD

d) BINARY - MAD

e) TD (T=5)

f) TD (T=5)

Figure 5.18 Scene 2, Vertical Profile, Gradient (Noise-free)

GRADIENT PROCESSING

BEFORE

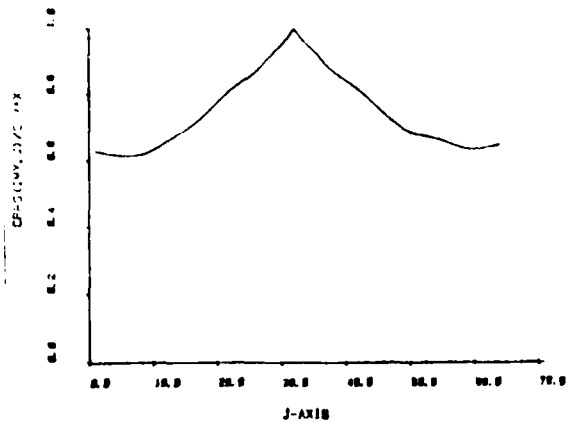

a) DCC 8-bit

AFTER

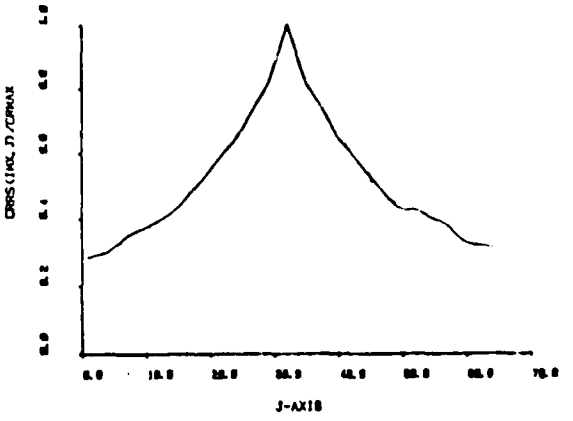

b) DCC 8-bit

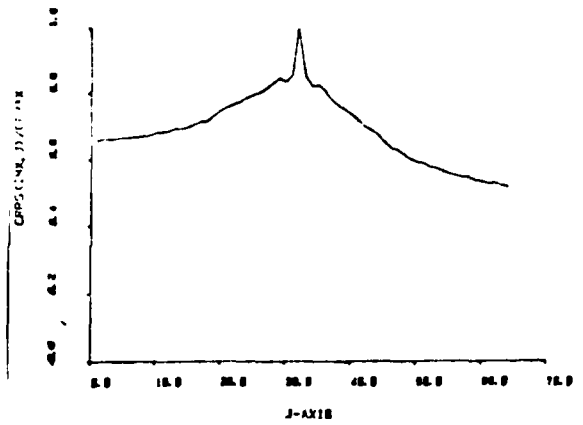

c) TRI-LEVEL DCC

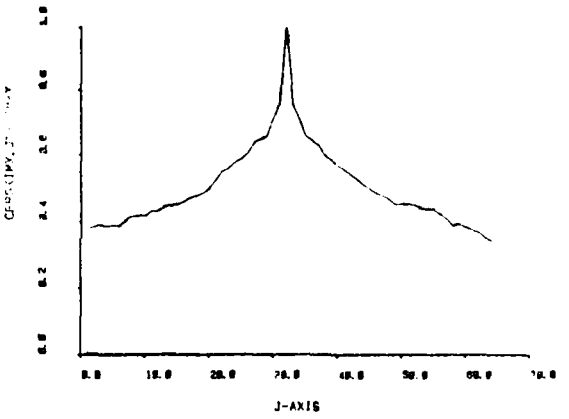

d) TRI-LEVEL DCC

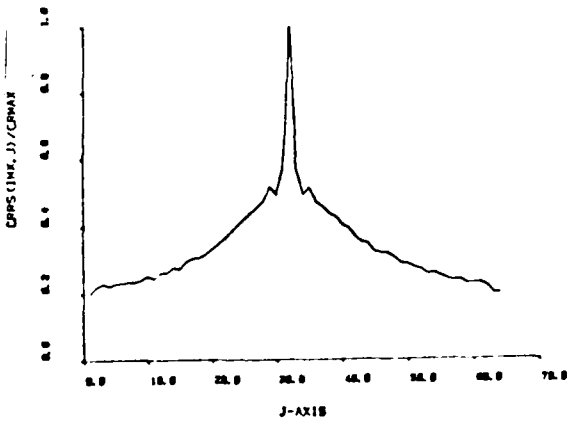

e) TD (T=5)

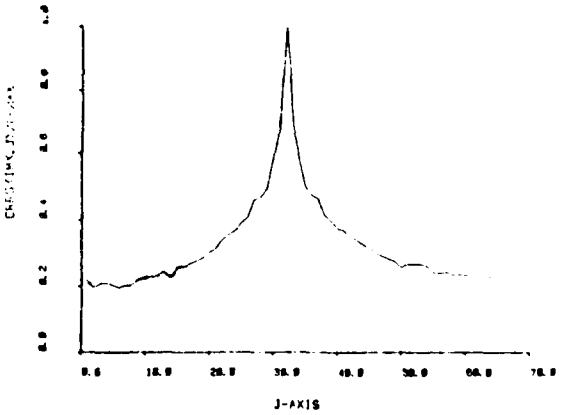

f) TD (T=5)

Figure 5.19 Scene 2, Horizontal Profile, Gradient (Noise-free)

correlation function. For binary quantization the MAD and DCC correlation metrics give equivalent results. Figure 5.20 shows the vertical cross-section through the peak for Scene 1. The a) part of Figure 5.20 gives the result without adaptive thresholding for comparison. The b) part shows the result for a 3 x 3 adaptive mean threshold with no noise. Parts c) and d) show the DCC and MAD adaptive threshold methods (mean threshold) for additive noise (SNR = 1.42); and parts e) and f) show similar results for a SNR = 0.43. Different profiles were obtained for DCC and MAD with additive noise because the noise was different for separate runs (although SNR was fixed).

Figure 5.21 shows peak profiles in a horizontal direction for identical conditions as in Figure 5.20. The high frequency characteristic of the adaptive threshold method is particularly well demonstrated by a comparison of the a) and b) parts of Figure 5.21. Since noise added on a pixel by pixel basis is inherently high frequency, the adaptive threshold method should exhibit increased noise sensitivity for the simulations with additive noise. This was verified by all simulations of the adaptive method with additive noise. A comparison of parts c) d) e) and f) of Figure 5.20 with Figures 5.14 and 5.15 b) illustrates the relative effects of noise on the adaptive threshold method.

Simulation results for a 3 x 3 adaptive median threshold are given in Figures 5.22 for the vertical peak profile and

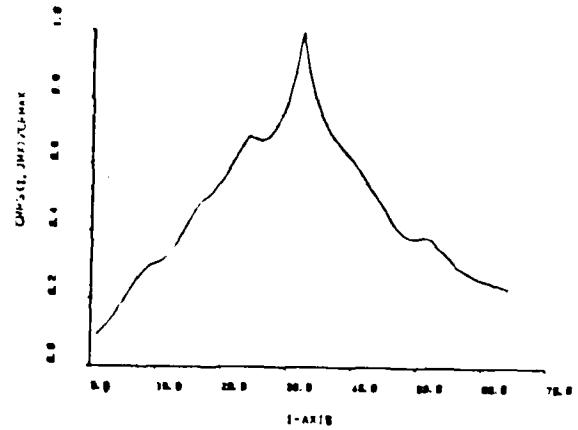

a) Binary, global
noise-free

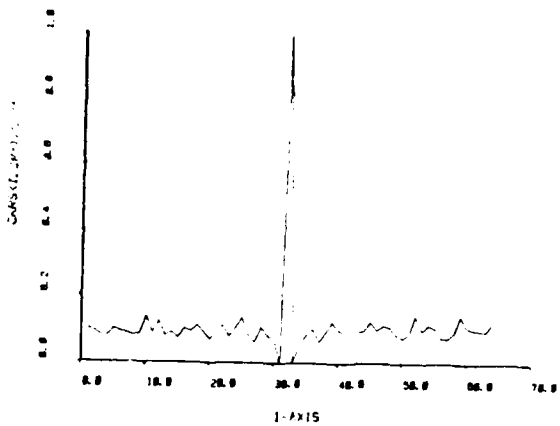

b) Binary, adaptive
noise-free

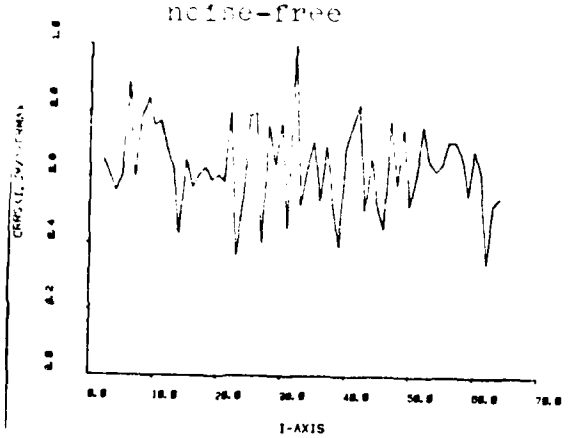

c) DCC adaptive Binary
SNR = 1.42

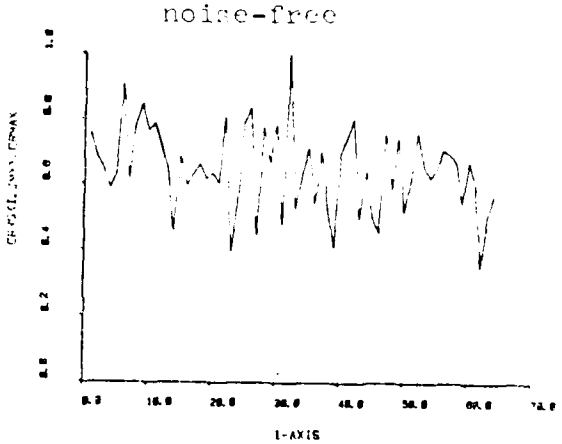

d) MAD adaptive Binary
SNR = 1.42

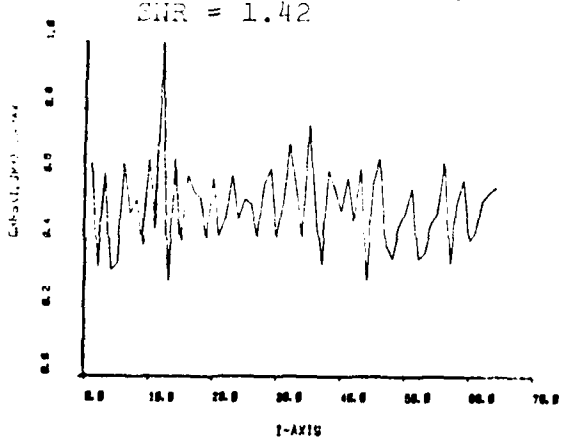

e) DCC adaptive Binary
SNR = 0.43

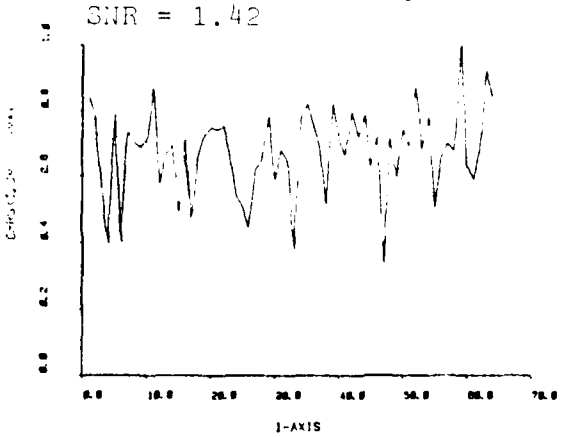

f) MAD adaptive Binary
SNR = 0.43

Figure 5.20 Scene 1 Vertical, 3 x 3 Mean Adaptive

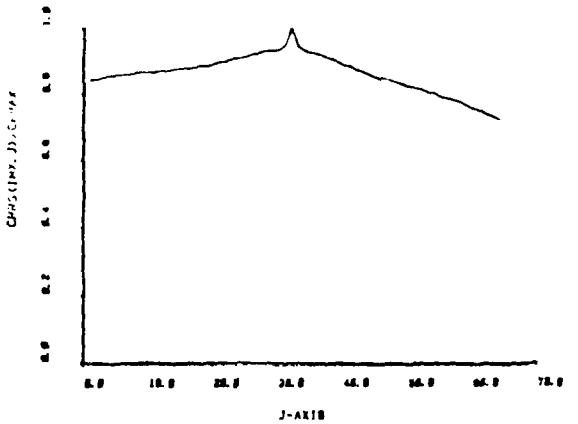

a) Binary, global noise-free

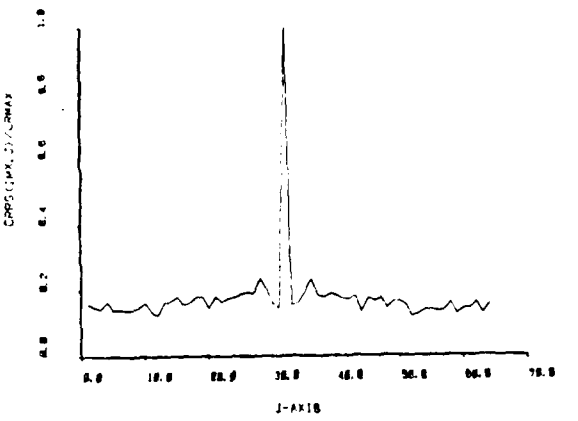

b) Binary adaptive noise-free

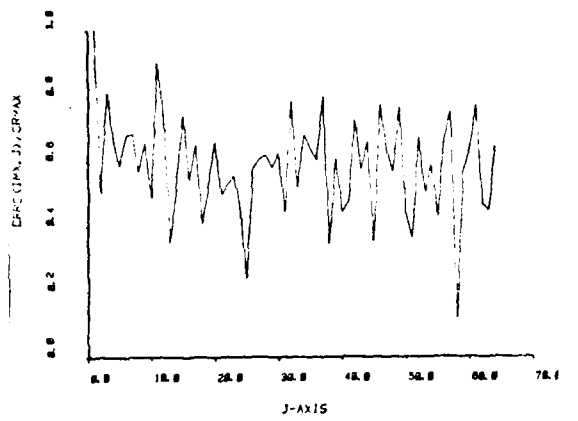

c) DCC adaptive Binary SNR = 1.42

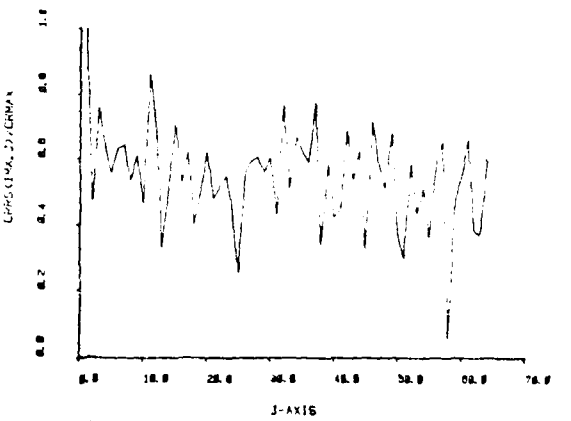

d) MAD adaptive Binary SNR = 1.42

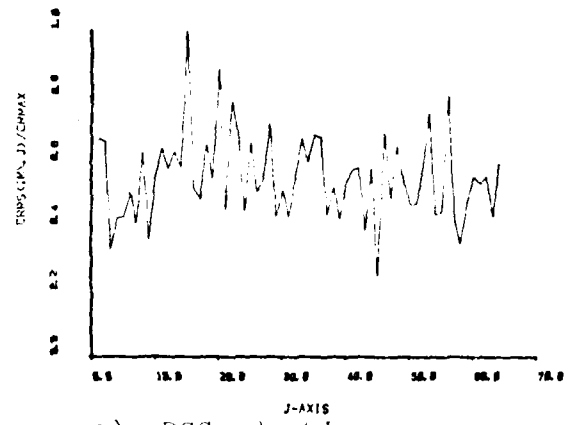

e) DCC adaptive Binary SNR = 0.43

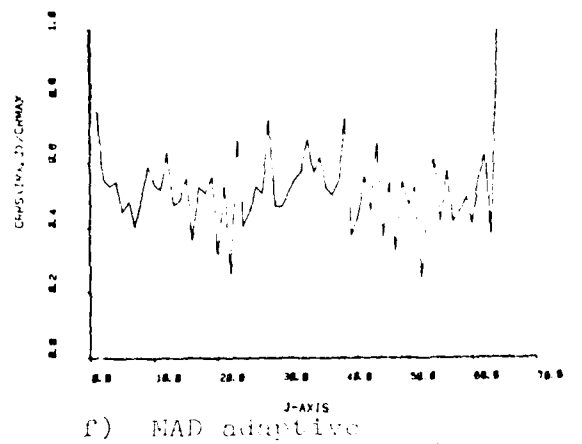

f) MAD adaptive Binary SNR = 0.43

Figure 5.21 Scene 1 Horizontal, 3 x 3 Mean Adaptive

5.23 for the horizontal peak profiles. In each figure a) gives non-adaptive result for comparison with b) the adaptive result without noise. Part c) is non-adaptive (SNR = 1.42) and d) is adaptive (SNR = 1.42). The noise effects on the high-frequency-emphasis adaptive threshold method is again verified by Figures 5.22 and 5.23. In fact, false peaks are evident. Table 5.3 summarizes the noise effects on the adaptive threshold method in terms of calculated peak locations.

TABLE 5.3

Noise Effects on Adaptive Threshold Method Peak Location		
Scene 1: Correct Peak Location = (32,32)		
	Mean Threshold	Median Threshold
Noise-Free	(32,32)	(32,32)
DCC(SNR=1.42)	(32,1)	(11,1)
MAD(SNR=1.42)	(32,1)	(11,1)
DCC(SNR=0.43)	(12,15)	—
MAD(SNR=0.43)	(59,64)	—

5.6 Non-Compatible Images. True cross-correlation simulation of non-compatible images was done for images with different spectral bands, different time of day and different scale. These simulations are described in this section.

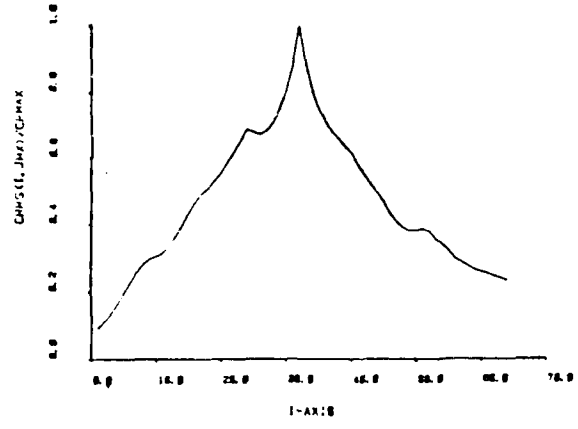

a) global
noise-free

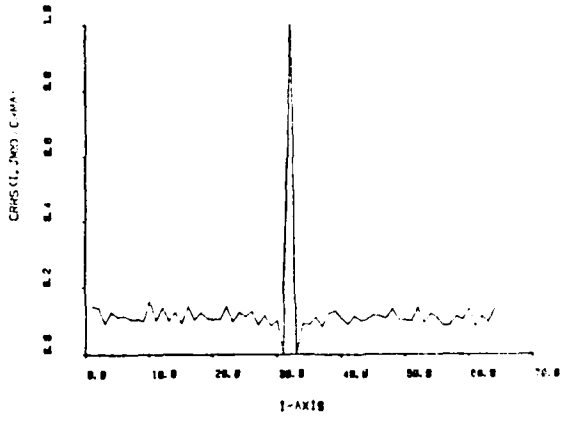

b) adaptive
noise-free

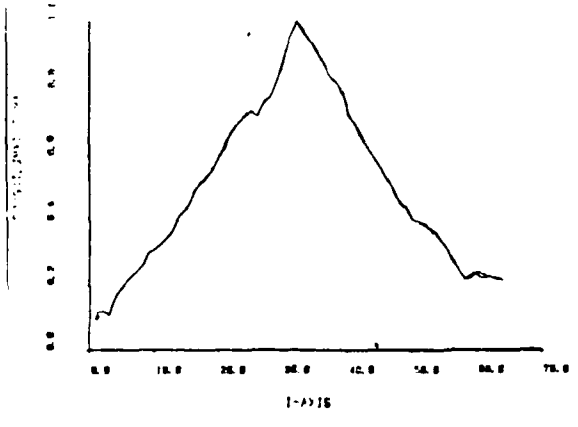

c) global
SNR = 1.42

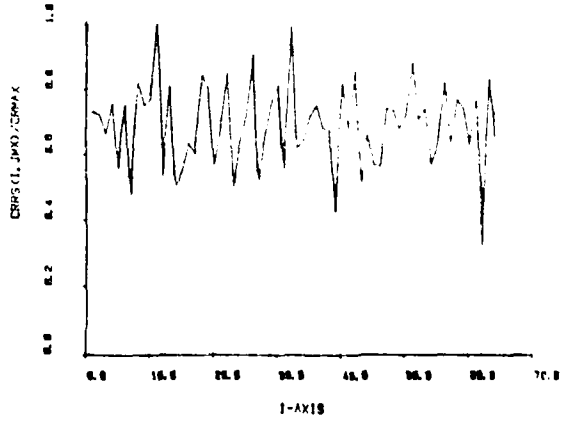

d) adaptive
SNR = 1.42

Figure 5.22 Scene 1, Vertical, 3 x 3 Median Adaptive

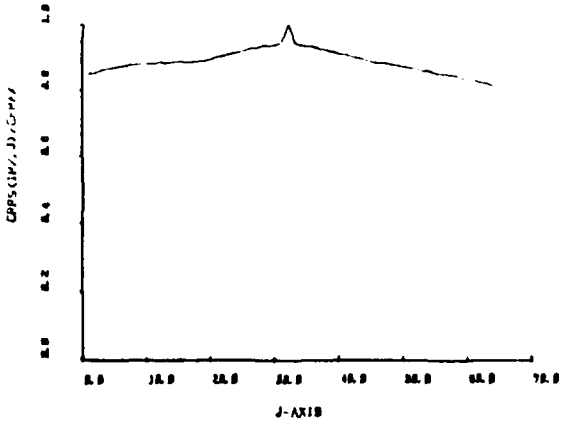

a) global
noise-free

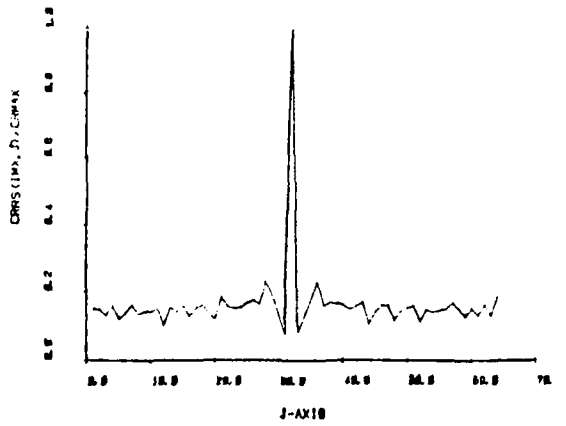

b) adaptive
noise-free

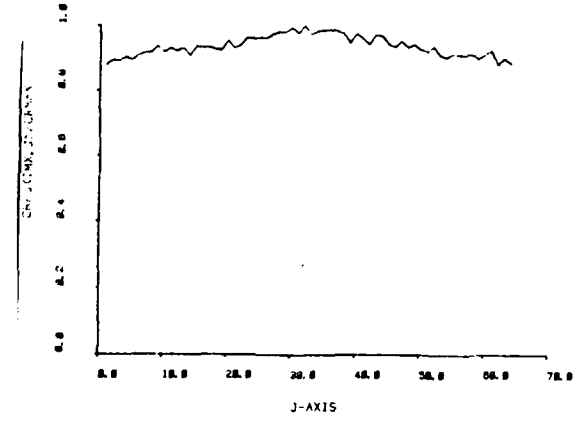

c) global
SNR = 1.42

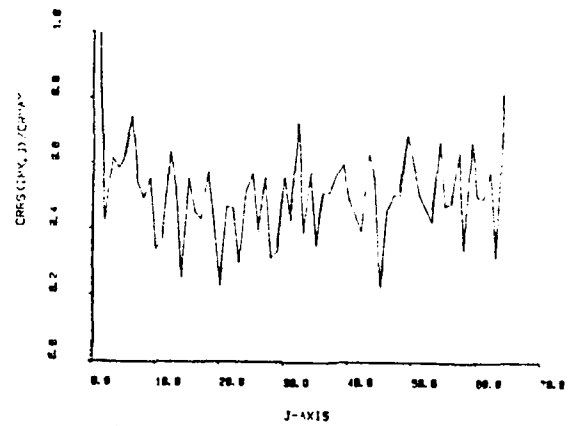

d) adaptive
SNR = 1.42

Figure 5.23 Scene 1, Horizontal, 3 x 3 Median Adaptive

5.6.1 Different Spectral Bands. Images listed as Ohio Files 26 and 27 in Table 5.1 were images of the same scene but in different spectral bands. Simulations were done to compare the DCC, MAD and TD registration methods with and without gradient preprocessing. A summary of the results is given in Table 5.4 in terms of computed registration coordinates.

TABLE 5.4

Results for Different Spectral Bands	
Images 7 & 8. Ohio File 26 (8-12μ) Ohio File 27 (Visible)	
Method	Registration Point
True Registration Point = (41,65)	
DCC 8 bit	(37,2)
MAD 8 bit	(40,29)
TD (T=10)	(41,29)
TD (T=50)	(41,29)
DCC 8 bit (Gradient)	(2,25)
MAD 8 bit (Gradient)	(2,51)
TD (T=10) (Gradient)	(41,50)
TD (T=50) (Gradient)	(4,32)

Clearly, the closest match is (41,50) for the TD (T=10) (Gradient) method. Yet the match is not accurate in the horizontal direction. This result indicates that further preprocessing to extract similarities between the two images is required.

The results are shown as profiles through the peak in Figures 5.24 and 5.25 for the unprocessed images and Figures 5.26 and 5.27 for the gradient images.

5.6.2 Different Time of Day. Images listed as Ohio Files 2 and 10 were infrared images taken at different times of day. These were used in cross-correlation simulations. Results are summarized in Table 5.5.

TABLE 5.5

Results for Different Time of Day	
Images 5 & 6. Ohio File 2 (Noon) Ohio File 10 (2:00 PM)	
Method True Match Point (51,51)	Registration Point
DCC 8 bit	(51,51)
MAD 8 bit	(51,51)
TD (T=5)	(51,51)
TD (T=10)	(51,51)
TD (T=15)	(51,51)
DCC 8 bit (Gradient)	(51,51)
MAD 8 bit (Gradient)	(51,51)
TD (T=5) (Gradient)	(51,51)
TD (T=10) (Gradient)	(51,51)
TD (T=15) (Gradient)	(51,51)

As can be seen all methods correctly indentified the registration point, so the best comparison of methods is in terms of relative peak sharpness and sidelobe levels.

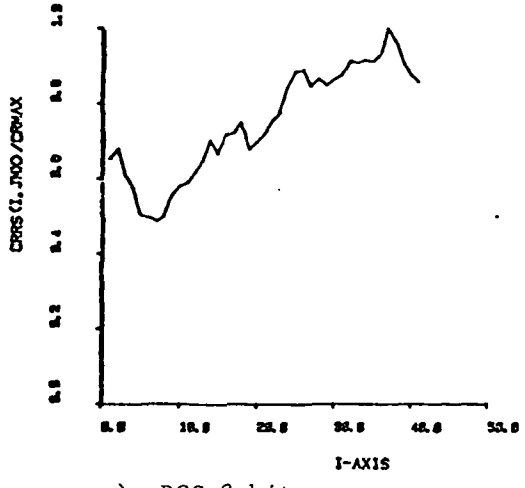

a) DCC 8-bit

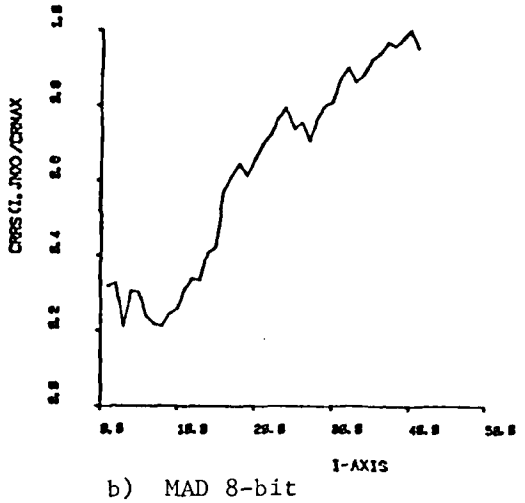

b) MAD 8-bit

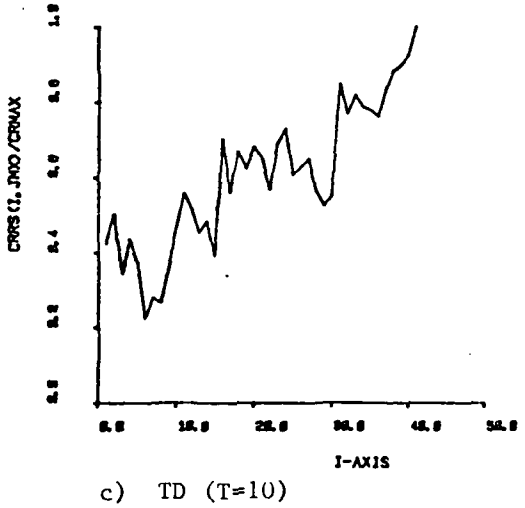

c) TD (T=10)

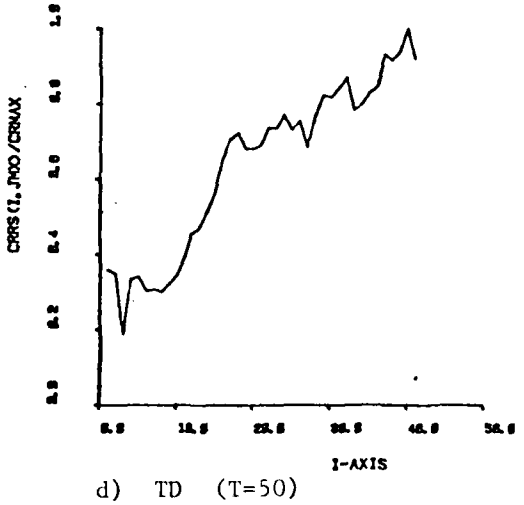

d) TD (T=50)

Figure 5.24 Different Spectral Bands (Vertical, Ohio Files 26,27)

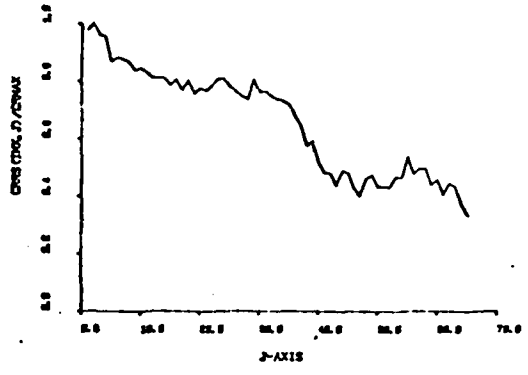

a) DCC 8-bit

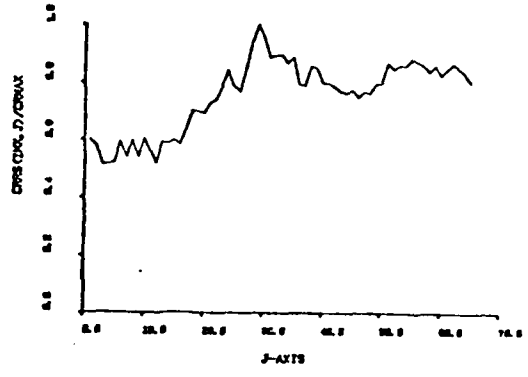

b) MAD 8-bit

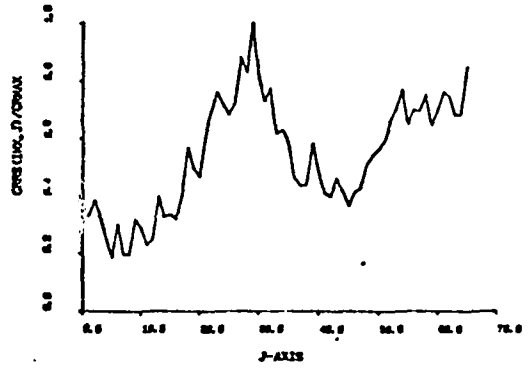

c) TD (T=10)

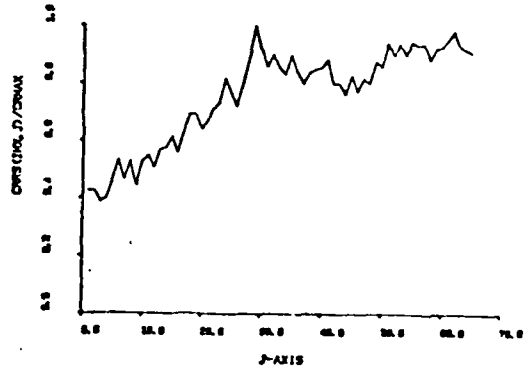

d) TD (T=50)

Figure 5.25 Different Spectral Bands (Horizontal, Ohio Files 26,27)

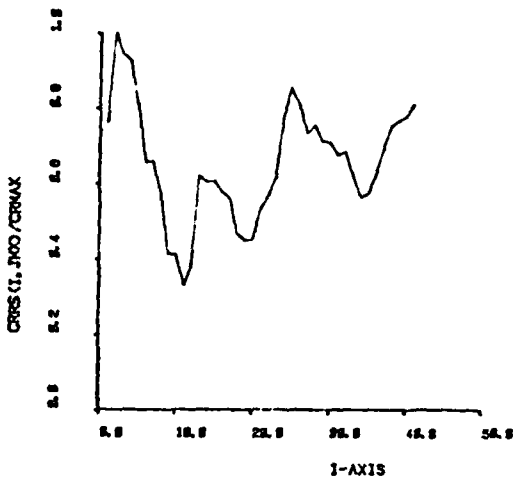

a) DCC 8-bit

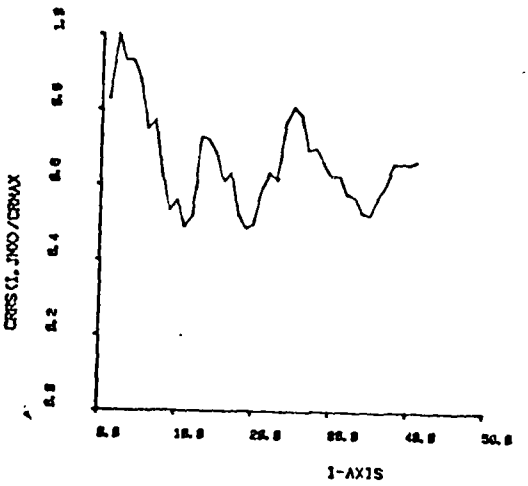

b) MAD 8-bit

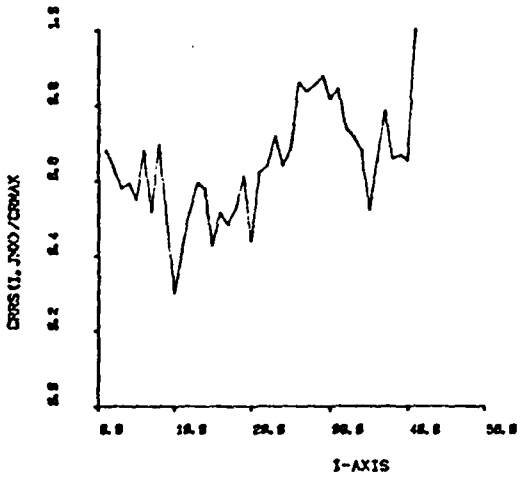

c) TD (T=10)

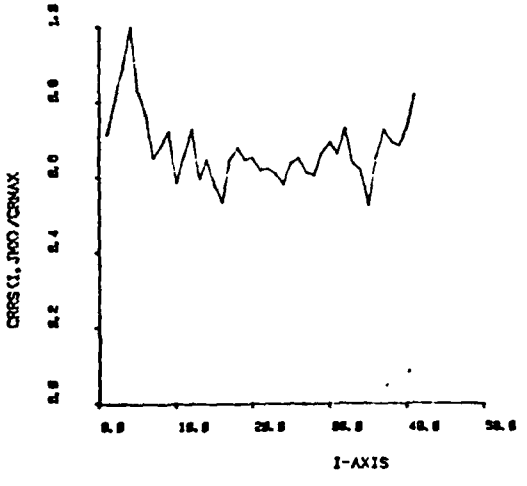

d) TD (T=50)

Figure 5.26 Different Spectral Bands, Gradient (Vertical, Ohio Files 26,27)

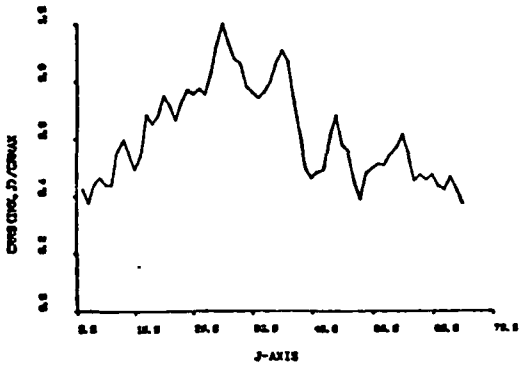

a) DCC 8-bit

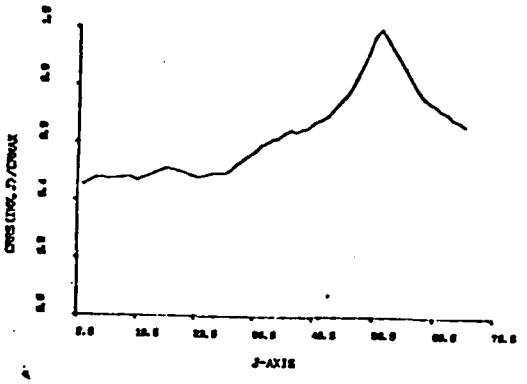

b) MAD 8-bit

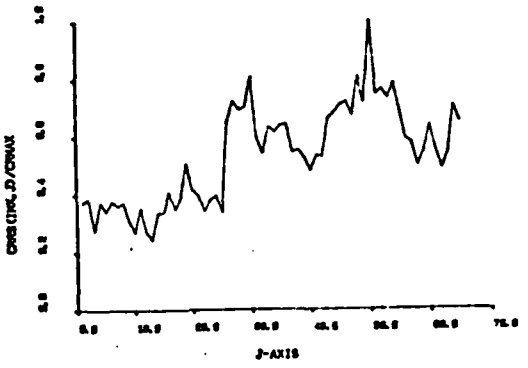

c) TD (T=10)

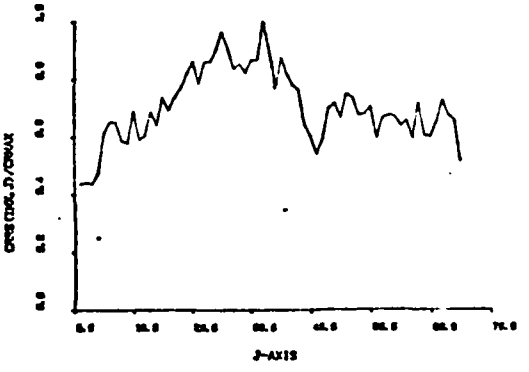

d) TD (T=50)

Figure 5.27 Different Spectral Bands, Gradient (Horizontal, Ohio Files 26,27)

Cross-sectional plots through the peak are shown in Figures 5.28 and 5.29 for the unprocessed images and in Figures 5.30 and 5.31 for the gradient images.

5.6.3 Different Scale. Images listed as HSV Files 9 and 10 in Table 5.1 were used in simulations of the cross correlation of images with different scale. Additionally, these two images were for different spectral bands. Results are summarized in Table 5.6 in terms of predicted registration point.

Peak profiles are given in Figures 5.32 and 5.33 for the unprocessed images. The DCC 8 bit, MAD 8 bit and TD (various thresholds) methods are compared. As can be seen from the Table and Figures, anamolous results were obtained for the TD method at low threshold values. This was expected becuase of the significant dissimilarity between the two images (different scale and different spectral band). It is significant that the TD method, with a suitably large threshold, performs as well or better than the DCC and MAD methods.

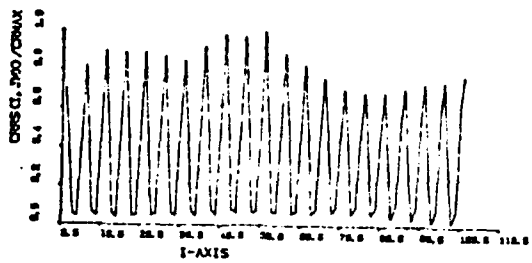

a) DCC 8-bit

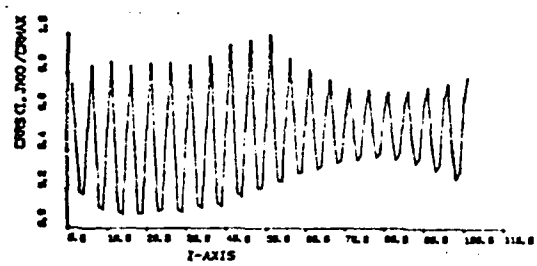

b) MAD 8-bit

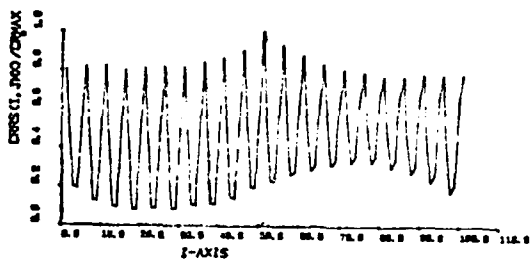

c) TD (T=5)

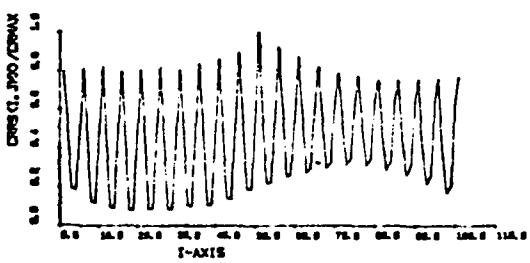

d) TD (T=10)

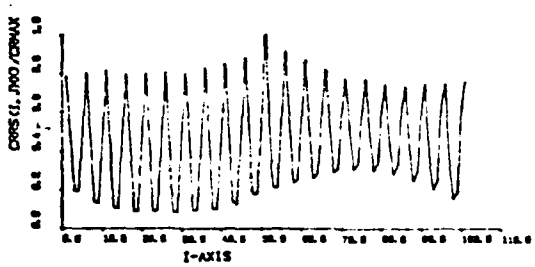

e) TD (T=15)

Figure 5.28 Different Time of Day (Vertical, Ohio Files 2,10)

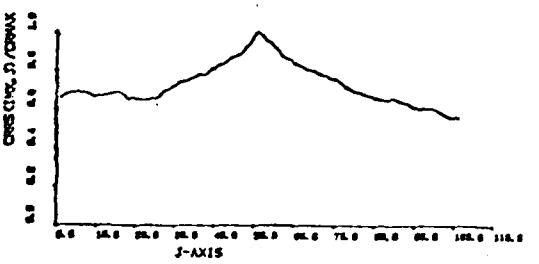

a) DCC 8-bit

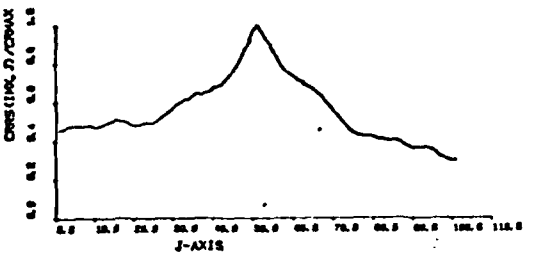

b) MAD 8-bit

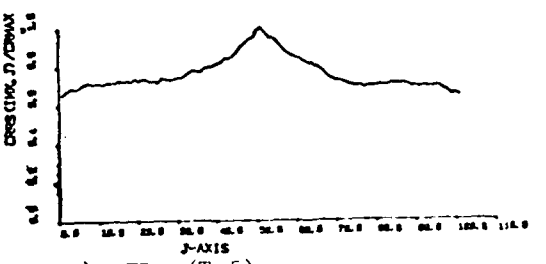

c) TD (T=5)

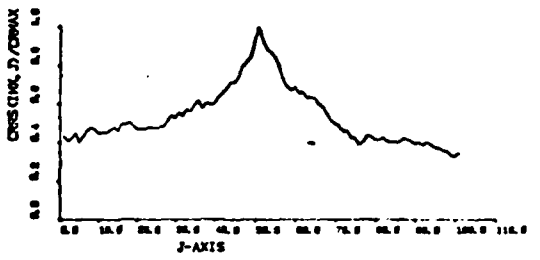

d) TD (T=10)

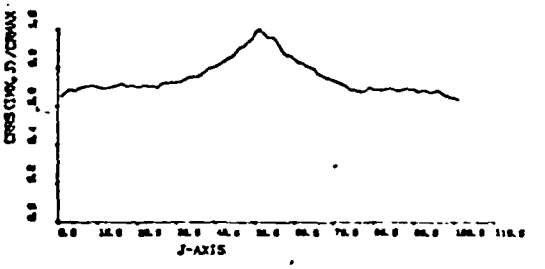

e) TD (T=15)

Figure 5.29 Different Time of Day (Horizontal, Ohio Files 2,10)

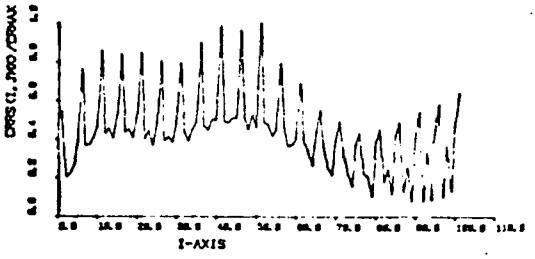

a) DCC 8-bit

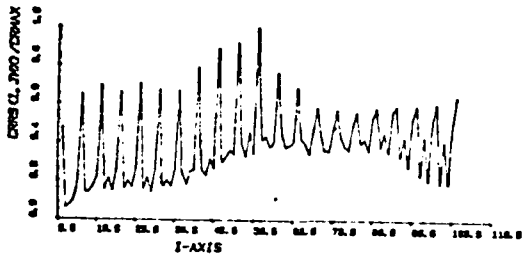

b) MAD 8-bit

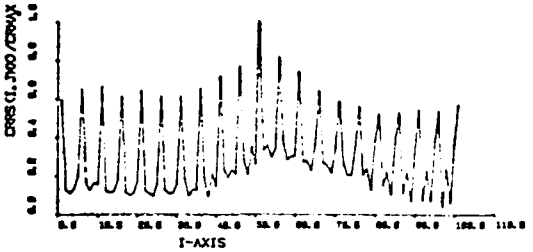

c) TD (T=5)

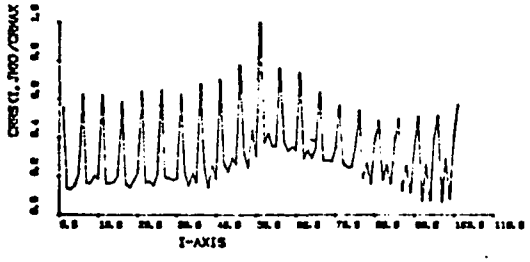

d) TD (T=10)

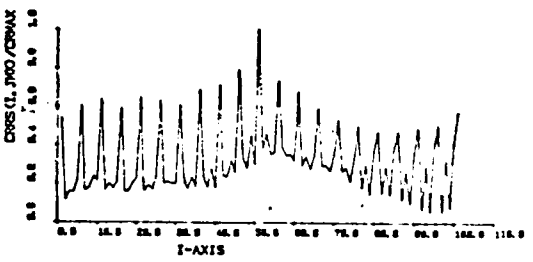

e) TD (T=15)

Figure 5.30 Different Time of Day, Gradient (Vertical Ohio Files 2,10)

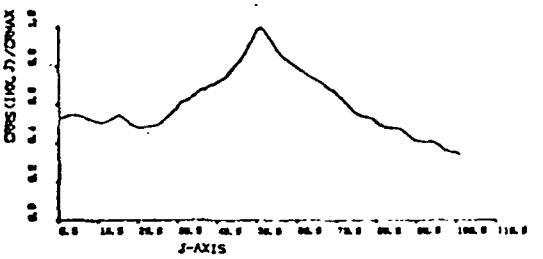

a) DCC 8-bit

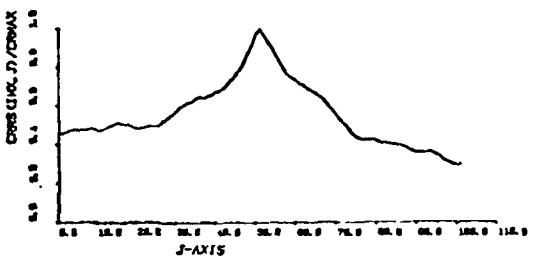

b) MAD 8-bit

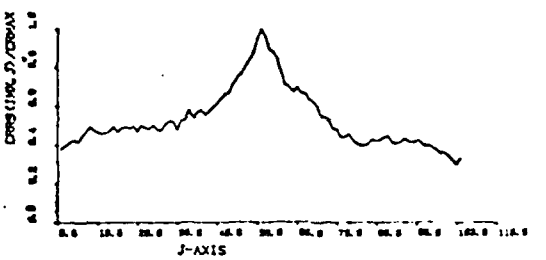

c) TD (T=5)

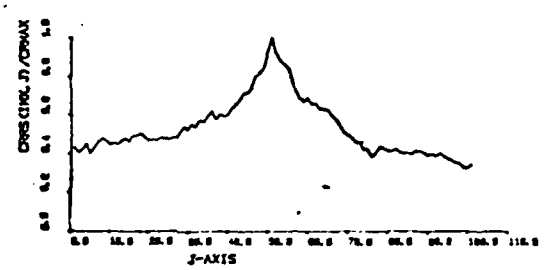

d) TD (T=10)

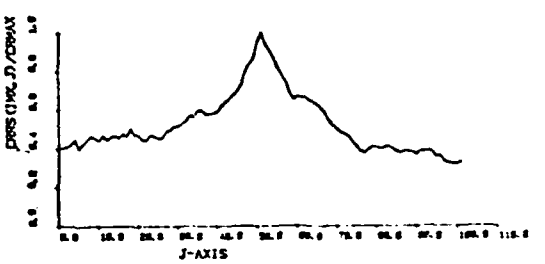

e) TD (T=15)

Figure 5.31 Different Time of Day, Gradient (Horizontal, Ohio Files 2,10)

TABLE 4.6

Results For Different Scale		
Images # 4 & 10:	HCV File 11 (BLUE MFLV) Scale 1.0 HCV File 4 (31 TV, MFLV) Scale .55	
Correct Match Point (11,6)		
Method	Peak Location	
	Unprocessed	Gradient
DCC 8 bit	(11,6)	(11,6)
MAD 8 bit	(11,6)	(11,6)
TD (T=5)	(41,28)	(44,44)
TD (T=10)	(43,25)	(44,45)
TD (T=15)	—	(45,44)
TD (T=20)	(11,5)	(11,6)
TD (T=25)	(11,6)	(11,7)
TD (T=30)	(11,6)	(11,6)
TD (T=35)	(11,6)	(11,6)
TD (T=40)	(20,46)	(11,6)
TD (T=45)	—	(11,6)
TD (T=50)	(41,44)	(11,6)

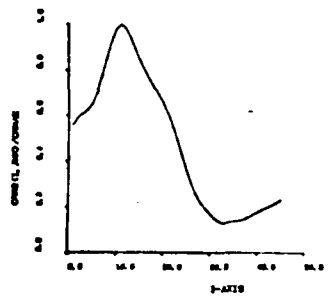

a) DCC 8-bit

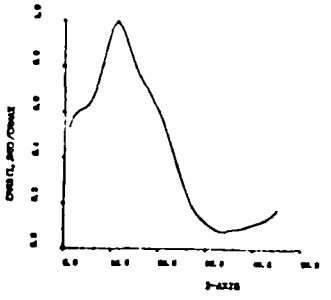

b) MAD 8-bit

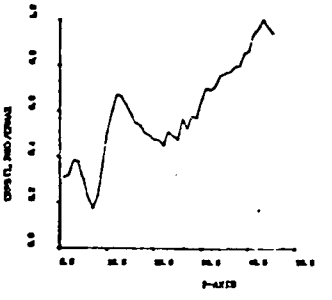

c) TD (T=10)

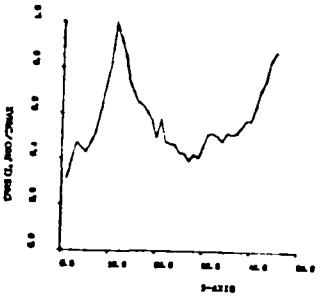

d) TD (T=20)

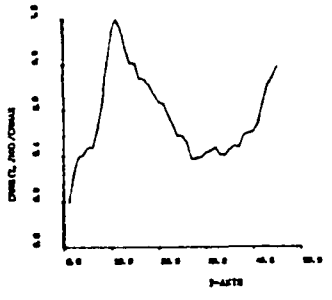

e) TD (T=25)

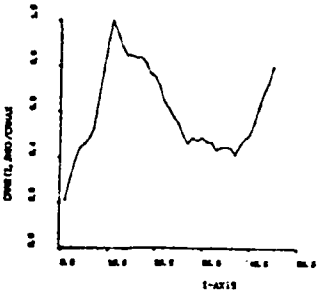

f) TD (T=30)

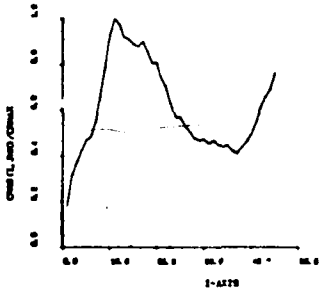

g) TD (T=35)

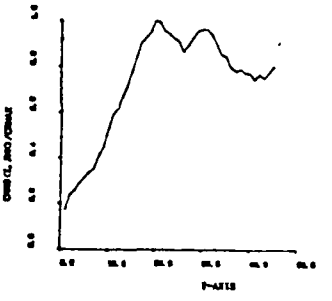

h) TD (T=40)

Figure 5.32 Different Scale & Spectral Bands (Vertical, HSV Files 10,9)

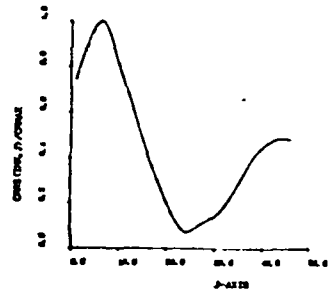

a) DCC 8-bit

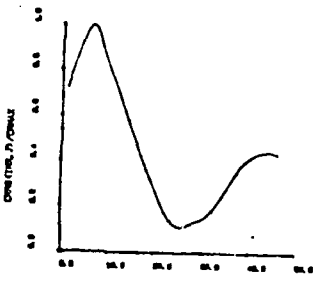

b) MAD 8-bit

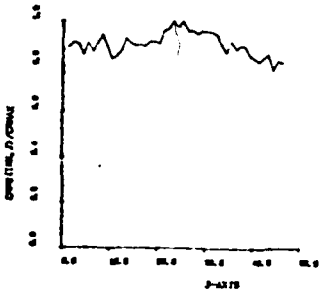

c) TD (T=10)

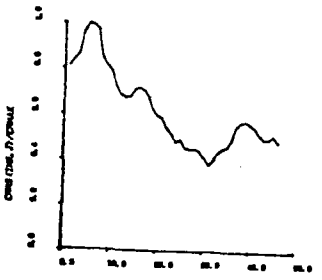

d) TD (T=20)

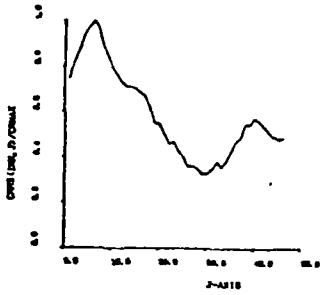

e) TD (T=25)

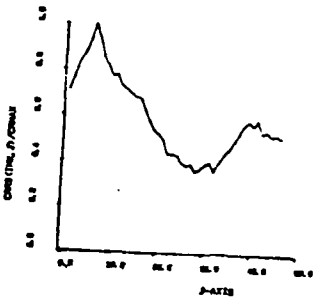

f) TD (T=30)

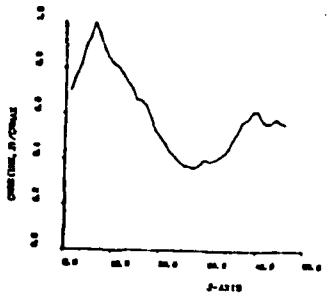

g) TD (T=35)

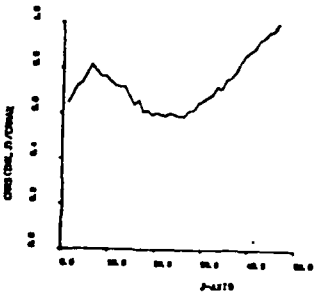

h) TD (T=40)

Figure 5.33 Different Scale & Spectral Bands (Horizontal, HSV Files 10,9)

CONCLUSIONS AND RECOMMENDATIONS

The most significant result of this effort has been the definition of a new registration metric (the thresholded difference method) which is adaptive to scene content. Comparison of the TD method with DCC and MAD for the Scene 1 and 2 vertical and horizontal directions (with significantly different frequency content) shows that for the ideal case (T=0) the TD method always gives a perfect correlation peak.

As the threshold (T) must be increased to allow for noise or image distortions, some of the advantage of the TD method is lost. However, with only a few exceptions (simulations which produced false peaks), the TD method was as good as or better than any other method. An optimum threshold for the TD method should be based on some measure of noise and/or distortion between the two images to be correlated. Further work is recommended to provide the theoretical basis and a practical measurement technique to establish an optimum value for T in a realistic application.

A single adaptive quantization method for the binary correlator was shown to give significant improvement in correlation peak sharpness. Unfortunately it showed high sensitivity to noise in the images. If the imagery to be correlated has low noise levels at higher spatial frequencies and if image distortions are strong only at low spatial frequencies then the adaptive quantizer offers superior registration performance over the global quantizer.

An overall accomplishment of this effort was the development of scene adaptive methods for improving image registration. The two methods described above offer potentially significant improvements in correlator performance, even though they have some shortcomings.

It is the opinion of the authors that further investigation and development of scene adaptive methods could make pixel-by-pixel registration methods more accurate and less sensitive to image distortions. Follow-on work in this area is recommended.

REFERENCES

[1] Daniel, I. Barnea and Harvey F. Silverman, "A Class of Algorithms for Fast Digital Image Registration," IEEE Transactions on Computers, Vol. C-21, No. 2, pp. 179-186, February 1972.

[2] C. D. Kuglin and D. C. Hines, "The Phase Correlation Image Alignment Method," Proceedings of the IEEE 1975 International Conference on Cybernetics and Society, Sep. 1975.

[3] B. F. C. Cooper, "Correlators with two-bit quantization," Aust. J. Phys., Vol. 23, pp. 521-527, 1970.

[4] W. R. Burns and Stanton S. Yao, "Clipping Loss in the One-bit Autocorrelation Spectral Line Receiver," Radio Science, Vol. 4, No.5, pp. 431-436, May 1969.

[5] F. K. Bowers and R. J. Klinger, "Quantization Noise of Correlation Spectrometers," Astron, Astrophysics, Suppl. 15, pp. 373-380, 1974.

[6] J. S. Boland, III, L. J. Pinson, G. R. Kane, M. A. Honnell and E. G. Peters, "Automatic Target Hand-Off Using Correlation Techniques," Final Technical report, U. S. Army Contract DAAH01-76-C-0396, 31 January 1977, 135 pages.

[7] E. G. Peters, J. S. Boland III, L. J. Pinson and W. W. Malcolm, "Quantization Effects on Signal Matching Functions", IEEE Trans. on Info. Thy., May 1978.

[8] L. J. Pinson, J. S. Boland III and W. W. Malcolm, "Statistical Analysis for a Binary Image Correlator in the Absence of Geometric Distortion", Optical Engineering, v.17, No. 6 Nov-Dec. 1978, pp. 635-640.

[9] Anthony J. Rockmore, "The Probability of False Acquisition for Image Registration," Presented at Symposium of Current Mathematical Problems in Image Science, Nov. 10-12, 1976, Monterey, CA.

[10] H. H. Bailey, F. W. Blackwell, C. L. Lowery and J. A. Ratkovic, "Image Correlation: Part I Simulation and Analysis", Rand Report R-2057/1-PR, Nov. 1976.

[11] J. S. Boland, L. J. Pinson, and E. G. Peters, "Automatic Target Handoff for Non-Compatible Imaging Systems", Final Report, Contract DAAK40-77-C-0156.

[12] L. J. Pinson, "Statistical Performance For a Digital Image Correlator-Scene Dependence", Final Technical Report, Contract DAAG29-76-D-0100, D.O. 1069, May 31, 1979.


DATE
FILMED
7-8